AUTONOMOUS SPACE PROCESSOR FOR ORBITAL DEBRIS
Final Report
(1989-1990)

Submitted by:

Dr. Kumar Ramohalli

David Campbell

Micky Marine

Mohamad Saad

Daniel Bertles

Dave Nichols

University of Arizona
Tucson, Arizona

ABSTRACT

This work continues to develop advaced designs toward the ultimate goal of a GETAWAY special to demonstrate economical removal of orbital debris utilizing local resources in orbit. The fundamental technical feasibility was demonstrated in 1988 through theoretical calculations, quantitative computer animation, a solar focal point cutter, a robotic arm design and a subscale model. Last year improvements were made to the solar cutter and the robotic arm. Also performed last year was a mission analysis which showed the feasibility of retrieve at least four large (>1500 kg) pieces of debris. Advances made during this reporting period are the incorporation of digital control with the existing placement arm, the development of a new robotic manipulator arm, and the study of debris spin attenuation. These advances are discussed here.

INTRODUCTION

We can hardly improve upon the lucid descriptions of the orbital debris issue, by science writers[1-4] and other popular news media coverage[5-9]. Without doubt, the problems of orbital debris have grown to be of serious concern to astronomers, space technologists and to terrestrial dwellers. The specific problems were presented at the XXXIX IAF Congress. The University of Arizona Space Engineering Design team is developing the design for economical removal of the larger debris pieces through local resource utilization. The fundamental idea is to concentrate solar energy into a point focus, cut the debris into precise shapes that can be added on to the "sweeper" craft and robotically assemble the pieces into a manageable configuration - to be followed by one of three disposal modes: (i) retrieval by a spacecraft (STS, HERMES, BURAN, etc.), (ii) precise ocean splashdown, or (iii) planned burnup upon atmospheric reentry. The fundamental space technologies to be demonstrated are solar cutting of candidate space debris materials, robotic assembly and accurate disposal. In 1988 the University of Arizona began participation in the USRA program and demonstrated solar cutting and a subscale model robotic arm. In 1989, a full scale robotic arm with manual controls was developed and the solar cutter/robotic arm assembly was shown to be technically feasible. Also in 1989, a mission analysis was performed in which the large debris environment was identified and a four debris retrieval sample mission analysis showed the propellant requirements to be well within reason. This year, 1990, the existing robotic arm was converted to digital control using an IBM PC, a second robotic arm was developed for precise pick and place operations and the problem of debris tumbling was addressed and various detumbling methods were investigated. This report is a summary of the work and explains the details of space engineering.

Consistent with the USRA philosophy, new undergraduate students were involved in the design process. This year, 11 new students were involved in the Autonomous

1

Space Processor for Orbital Debris (ASPOD) design. The project continues to draw worldwide attention including correspondence with elementary and high schools. Some of these are documented in the Appendix.

DEBRIS SPIN ATTENUATION

The purpose of this project was to research and recommend methods of attenuating the rotational spin of orbital debris so that ASPOD satellite can safely grasp them for retrieval. To avoid possible damage to the ASPOD craft, only passive means of attenuation were investigated. The use of passive means is defined as the use of methods of attenuation which do not involve ASPOD in direct contact with space debris therefore endangering it. Some of the design criteria and target specifications are outlined below:

- Attenuate the rotation of an object spinning about one axis.
  (see Appendix A for details of satellite spin stability.)
- Attenuate the rotation of an object having a mass of up to 2000 kilograms
   and rotating with rotational speeds of up to 50 revolutions per minute
- Attenuate the rotation of an object up to 7 meters in diameter and up to 7
   meters in height
- Use a minimal amount of energy
- Attenuate at least 4 objects per mission
- Require no maintenance
- Must not interfere with the normal operation of other functional satellites
- Must not create more debris
- Must weigh less than about 500 pounds
- Must have a reasonable expense relative to the space industry

Satellites and most other space debris generally contain a certain amount of rotational energy. The problem of dealing with the rotation of a large, nonsymmetric object containing a lot of mass orbiting the earth must be solved before the satellites can be safely and effectively collected.

A workable solution dealing with debris capture must allow the rotational energy of the debris to be contained or dissipated without transferring it to the collector satellite. The space debris that is proposed for collection is often very massive, 2000 kilograms or more, with spin rates of up to 50 r.p.m.. These figures suggest that there can be quite a bit of angular momentum involved.

SOLUTIONS

As a first step, various attenuation methods were researched and evaluated. Of all the methods investigated four were chosen as possible solutions and merited further analysis. Each of these four solutions uses a different physical principle, for example, conservation of angular momentum or conservation of energy, to accomplish the attenuation of the satellite.

Although each of the four designs merit further investigation, for the present the most promising of the four was singled out for detailed analysis and testing.

A)   Reeled Weight Mechanism

The physical principle used in this method is to translate the rotational energy into linear kinetic energy, then into potential energy. This design uses a reeled cable capable of attaching itself to the debris by the cable's free end. Also contained in the reel mechanism is a generator allowing the cable to reel out, turning permanent magnets around a stationary armature and storing that energy in a battery. This generator can then act as a motor by turning the stored energy in shaft power, allowing the cable to be reeled in. Once the free end of the cable is attached to the debris in its plane of rotation, the reel is then allowed to freely move away from the debris due to centrifugal acceleration, yet is still tethered by the cable. The reel will move away in a straight path while the debris continues to spin and the attachment point of the cable on the debris will rotate with the debris, wrapping a portion of the cable around the debris. At this time the reel will create a drag force on the cable by engaging the generator and then storing that energy. Due to the centripetal force of the reel attached to the much more massive piece of debris, the reel will attempt to move into a radial position about the debris' center of mass. Before it comes near this point some of the stored energy will be used to reel the reel mechanism back into the debris, at which point the process will start over. Some of the advantages to this system are the ease of attachment to essentially any shape of debris, and the relative simplicity of the mechanism. Some of the problems are the difficulty in analysis and testing of the system and the chance of the cable becoming permanently entangled in protrusions on the debris.

B)   Coiled Spring Mechanism

Figure 1 presents the proposed configuration for the coiled spring mechanism. This proposed mechanism consists of a component for attaching to the debris, a ratchet, a coiled spring and a stabilizer. The idea behind this solution, is to absorb the rotational energy of the debris and store it in a coiled spring as potential energy. The purpose of the ratchet is to act as a locking mechanism for the spring when it winds up completely. Winding up the spring though, necessitates the use of a stabilizer to hold the other end of the spring fixed. A stabilizer is thought of as a servo-controlled gyroscopic platform where gyroscopes are to be used only as sensors. The resolver (the "brain" of the control system) will be continually feeding corrections through the feedback controlled-loop to keep the attachment to the platform fixed in space. The greatest advantage of this process is that it can attenuate the rotation of the debris quickly, within minutes (see Appendix B). Furthermore, the attenuation of the debris is complete (100%). The disadvantages of this idea are the requirements for powering the gyroscopic sensors and lubricating the ratchet. Another more important problem is that the ASPOD will eventually be involved actively in the process by powering several thrusters as well as

4

its momentum-wheels. since this may create safely problems for the vehicle itself, the idea was abandoned for the time being and our effort was concentrated on developing passive means of attenuation.
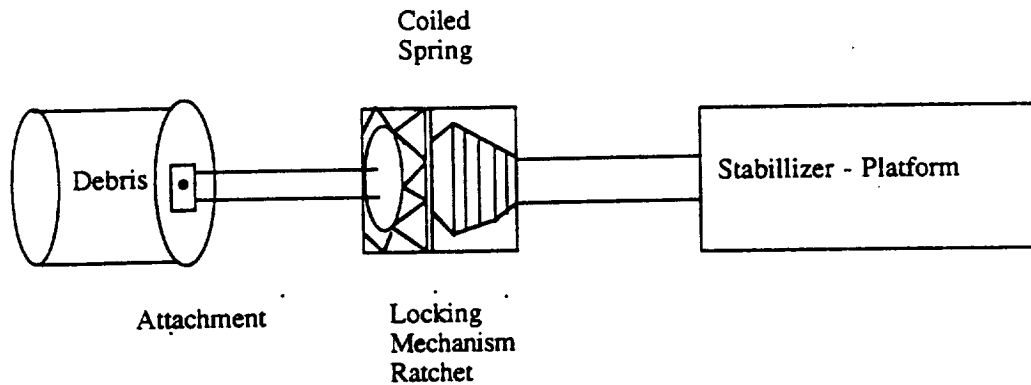
Coiled
Spring

Figure 1. Coiled Spring Mechanism

C)   Long Cable Mechanism

For this design there are two ways in which it could work. One would be to let out a cable with a mass attached to the end, thereby increasing the moment of inertia, and slowing the satellite down. This would not allow the satellite to some to a complete stop but it could possibly slow the satellite down enough for a robotic arm to manipulate it. The cable would have to be cut off when maximum attenuation occurs, preferably so that it would reenter the earth's atmosphere, because once the robotic arm attached to the satellite the cable would reel in uncontrollably due to the momentum of the cable. The other method would be to leave the cable on for an extended amount of time and allow the gravity gradient to slow the satellite to a complete stop. The satellite could then be grabbed and the cable reeled in since the rotation of the satellite would be fully attenuated. Figure 2 shows a representation of this method.
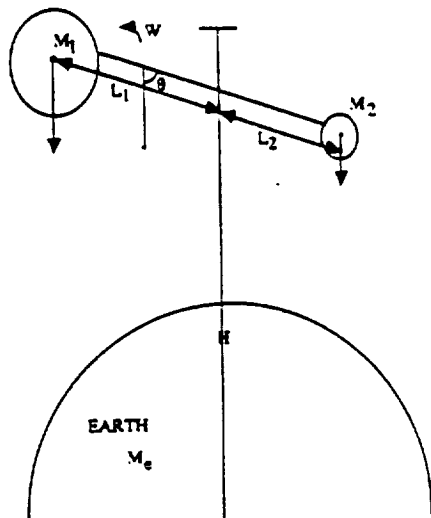

Figure 2. Long Cable configuration

5

D)   Geared-Bar Mechanism

The geared-bar mechanism is the solution recommended selected by the attenuation research group for further development and is detailed below.

GEARED-BAR MECHANISM

A)   Theory of Operation

A representation of the gear bar can be seen in Figure 3. The centrifugal acceleration acting on the flywheel, forces the flywheel radially outward to the end of the geared-bar. If the geared-bar was smooth, the flywheel would just translate outward without spinning, however, the contact forces between the gear and the bar apply a torque about the center of the gear forcing the flywheel to spin as well as translate. Mathematical analysis (see Appendix D) and experimentation shows that as the angular rotation of the flywheel increases, the angular rotation of the debris decreases. A ratcheting mechanism is attached to the system so that when the flywheel reaches the end of the bar the flywheel will continue to rotate freely.
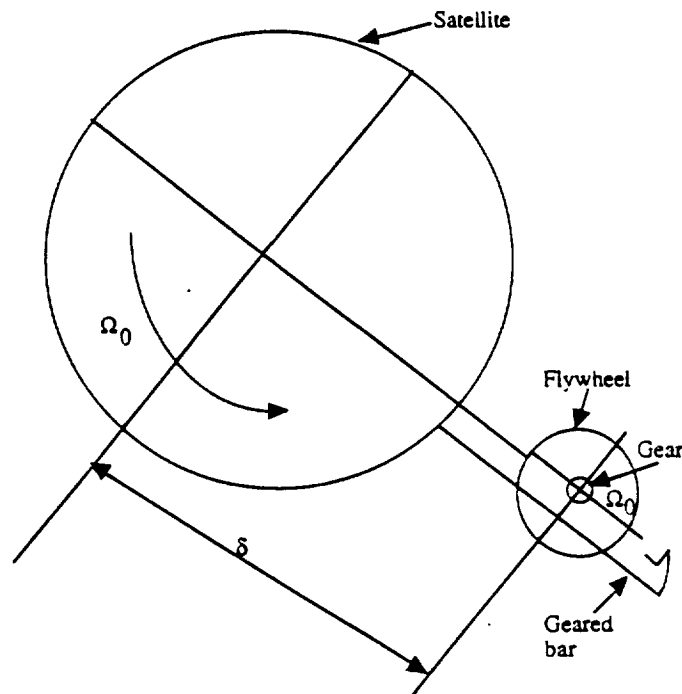

Figure 3. Geared-Bar Mechanism

The effectiveness of our design depends on the length of the geared-bar and the mass moment of inertia of the flywheel. It could happen that the configuration necessary to achieve an adequate amount of attenuation would be unfeasible to take into space due to

the size and/or mass of the flywheel and the length of the bar. If this is shown to be true it chould be possible to attach a motor to the flywheel and "reel" the flywheel back in, while the ratchet mechanism allows it to maintain its angular velocity, and let it move out again. This process could be repeated as many times as necessary.

B)   Design

A rudimentary device was fabricated for experimental purposes. The design that was used included a rubber wheel and friction bar to simulate the rack and pinion system. A small cart supporting the flywheel and friction wheel with a bearing rolled along a track that represented the geared-bar. The friction wheel rolled along a friction bar attached to the track forcing the flywheel to rotate. The combination of the flywheel and the cart simulated both the rotation and the translation of the flywheel.   To simulate the ratcheting mechanism, the friction bar was cut shorter than the track. This allowed the flywheel to rotate freely once it reached the end of the track. This design was not adaptable to the use of a motor; however, it was felt that showing that the theory mechanism would work for one pass was sufficient to show that this method of attenuation was feasible.

C)   Experiment

Previously, a large model representing space debris was built for attenuation experimentation purposes. This model is an octagonal solid approximately 48 inches in diameter and 72 inches high with a calculated mass moment of inertia of 655 lbm ft. The "debris" is attached to the ceiling and floor with a large metal rod that it rotates about. Lubricated bearings were used to minimize the frictional effects.

To gather data, a systematic process had to be developed to measure the time per revolution. A computer program was used to record the needed data. A mark was made on the "debris" and then the debris was spun up to an appropriate speed. Each time the mark came into sight, a key was pressed on the computer. The program would then print the number of the revolutions and measure the time elapsed. With this data, the program calculated the time between revolutions and revolutions per minute for each revolution. Finally, this data was exported to a spreadsheet program for further analysis and graphing.

To prove the effectiveness of the geared-bar mechanism, it was necessary to find a way to separate the effects of the changing mass moment of inertia, due to the flywheel translating outward versus the effects of the rotational kinetic energy being transfered to the flywheel. To do this, reference data had to be taken. This reference data consisted of several measurements with the flywheel retracted, and several with the flywheel extended.   Before measurements could be taken with the geared-bar mechanism fully operational, one additional component needed to be added.   Because

the debris needed to be brought up to a functioning speed before the flywheel could be released, it was necessary to develop a release mechanism so that the flywheel would not begin to move before the appropriate speed was attained. This was done by including an eyelet on the flywheel, and passing a pin through it that could be easily pulled out when needed without significantly effecting the speed of the debris.

As stated above, these measurements were taken for each case, the flywheel retracted, extended, and operational. Figures 4, 5, and 6 show the relative quality of the measurements for each case and their characteristic curves.
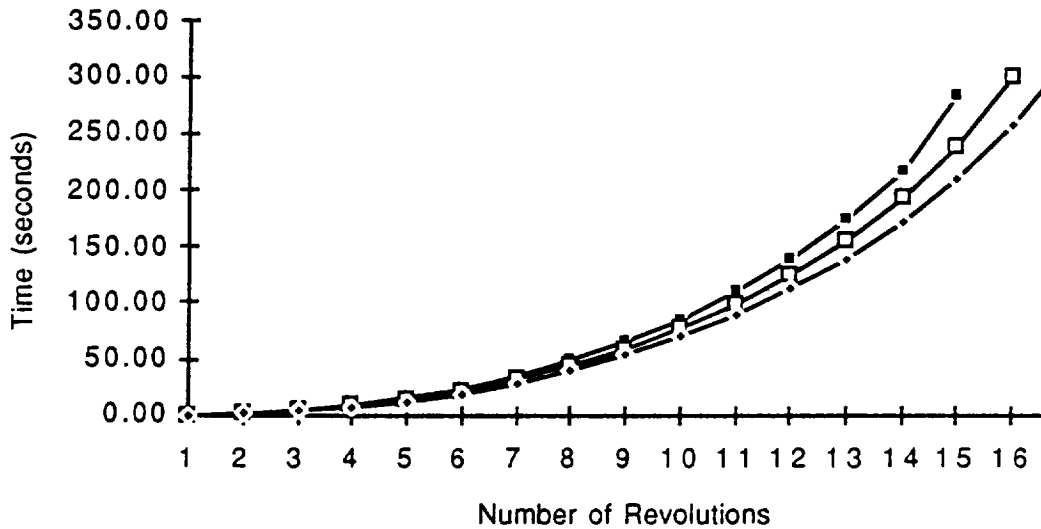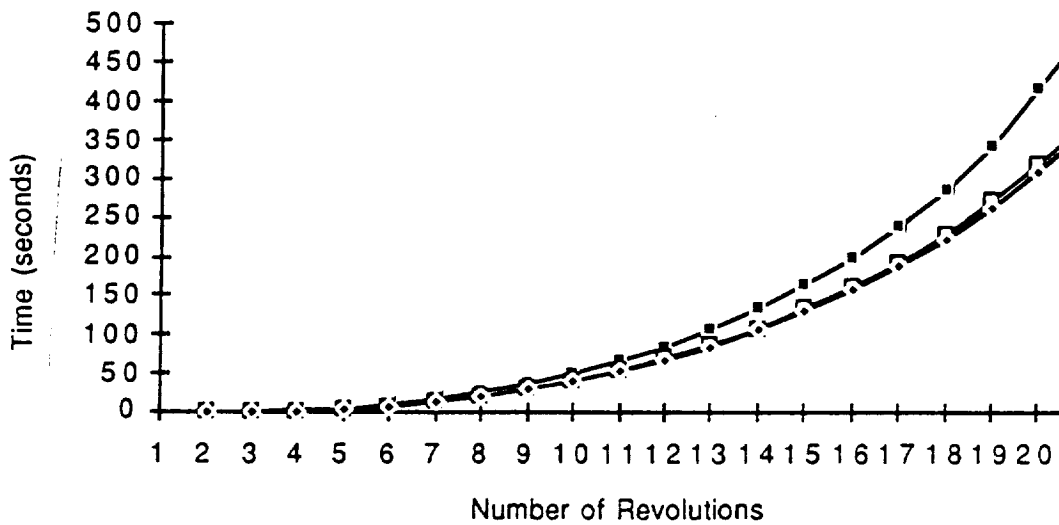
Figure 4. Flywheel Retracted
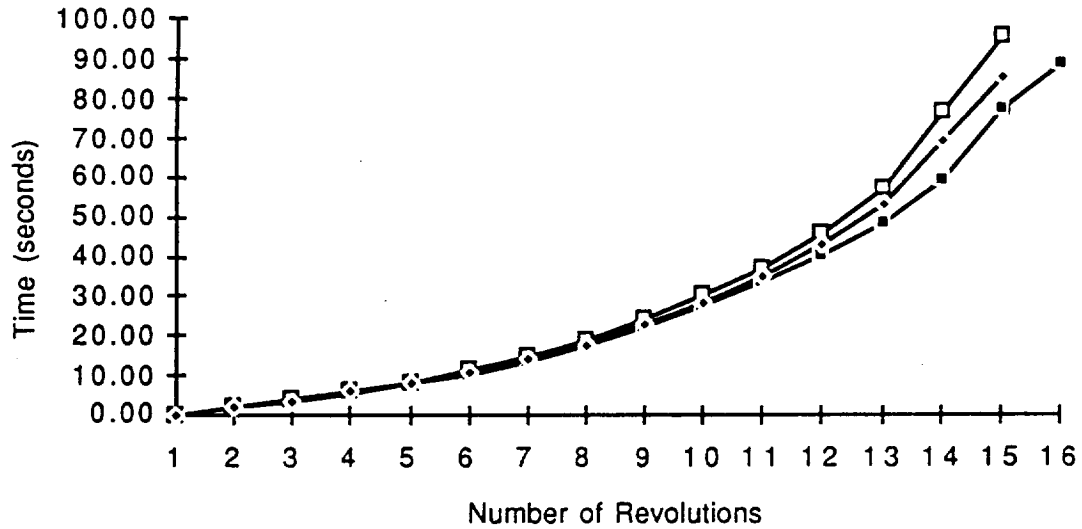
Figure 5. Flywheel Extended

Figure 6. Flywheel Translating

Although the reference data was taken, a standard procedure to spin up the debris at an equal RPM for each run was not developed, nor was there a way to measure the energy added to the system. It was, therefore, necessary to determine a method for comparing the data with the three different cases. Because of limitations with the graphing software used, it was felt that taking the points at which the debris came to rest with each case and counting the maximum, common number of data points backward would be a reasonable method for developing a common reference. For example, the working case only included 14 data points, so the last 14 data points for each case were used.

Figure 7 illustrates the effects between the three different cases. The line with the flywheel retracted is steep due to the low relative inertia. The line with the flywheel extended is flatter and the time of rotation longer due to the effects of increased mass moment of inertia. If the working case decreased the rotational speed of the debris solely due to the effects of the changing mass moment of inertia, one would expect the line for the working case to lie somewhere between the retracted and extended cases. In fact, the graph should begin at the approximate point of the retracted case because of the identical value for the mass moment of inertia and end near the same point of the extended case because the same amount of energy should still be in the system. It was not the groups goal to "prove" the effects of changing the mass moment of inertia, but to prove that the flywheel actually absorbs the energy of the debris. To confirm this, the graph of the working case should start near the point of the retracted case and end significantly below the extended case. The working case line does follow this hypothesis.
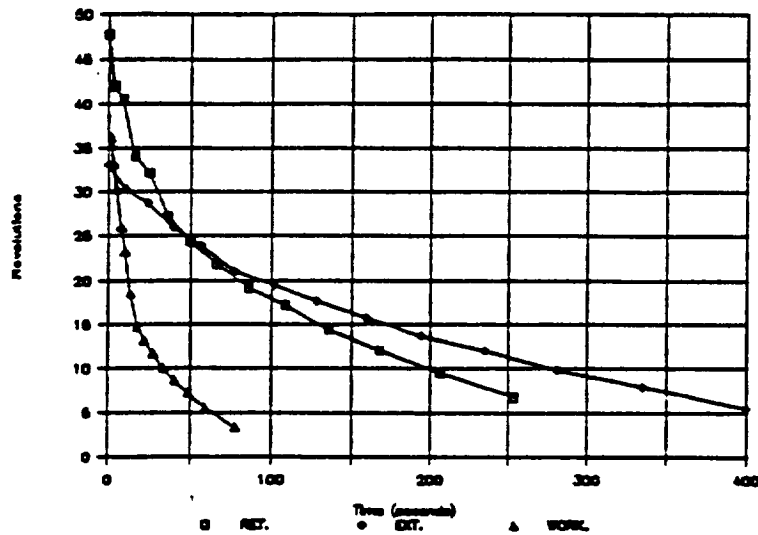
9

Figure 7. Experimental Comparison

This experiment does not exactly model the case of debris spinning in space because satellites in space are not pinned, therefore the center of rotation would change as the flywheel moves out. The mass of the flywheel could be optimized to minimize these effects. Nonetheless, this system of attenuation will still work, because the center of rotation will always lie between the centers of the debris and the flywheel, maintaining the centrifugal component of acceleration moving the flywheel outward.

In conclusion, and most importantly, the geared-bar mechanism of the experimental case does absorb the rotational energy of a spinning body. For the three cased mentioned above, the time for the last 14 data points is 253 second for the retracted case, 400 seconds for the extended case, and 59 seconds for the working case. The above experiment also proves that the attenuation is not solely due to the change in mass moment of inertia but actually performs a significant amount of energy transfer.

D)   Computer Modeling

In order to investigate the dynamics of the geared-bar mechanism, as an attenuator of the rotational energy of a satellite, several approximations to the actual case were considered. The first case, consisting of the two-dimensional analogue (Figure 8) of the actual case (Figure 9), assuming perfect targeting and neglecting the attachment phase and the endpoint locking of the flywheel, was solved analytically and appears in appendix D.
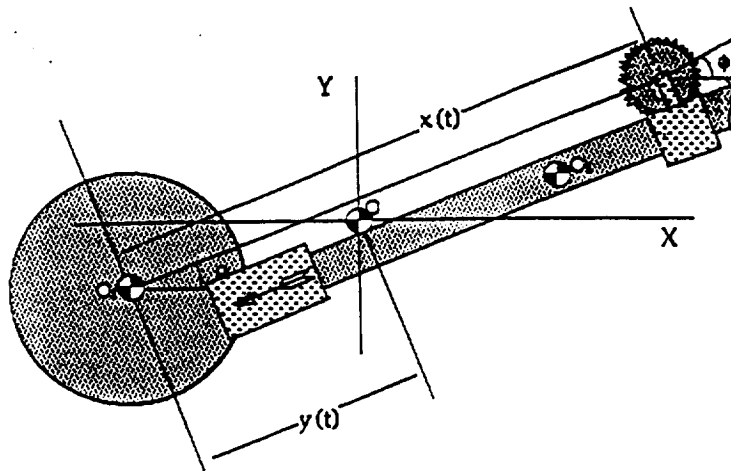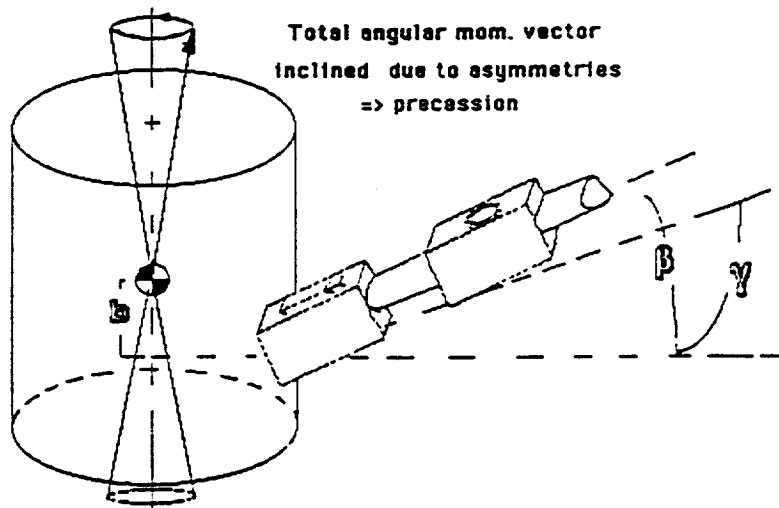
Figure 8. Attachment Parameters

Figure 9. Attachment Sensitivities

Under the above assumptions, the analysis suggested that an attenuation of about 50% could be attained for a rack length of 4 meters, and an operation of 50 seconds. These results pertain to a satellite modelled as a 2000 kg cylinder, 4 meters in height and 3 meters in radius rotating at 50 rpm. The 40 kg flywheel used in the analysis was 1 meter in diameter, while the rack was assumed weightless. At this point it should be mentioned that the attenuation effects are highly dependent on the inertial properties of

the satellite. Thus, it should be kept in mind that the diversity of satellites to be attenuated adds to the complications and limits the applicability of the design.

In order to investigate the effects of the geared-bar attenuator when it is not attached at right angles to the principal axis of rotation of the debris, as well as when it is attached off center with respect to the satellite' s center of mass (Figure 9), an analysis was attempted on a software package available at the University of Arizona. A copy of the parameters for the program can be found in Appendix E. This software facilitated a three dimensional analysis and made it possible to animate the resulting effects, for visual and demonstrational purposes. For a satellite with inertial properties as mentioned above, the software shows attenuation as high as 70% during the first 5 seconds for the two dimensional case, but not more than 25% for the three dimensional case that involves geometrical asymmetries and precessions. The fact that the rack and pinion joint is not 100%, as was assumed by the software, will lengthen the time needed for attenuation. Figures 10 and 11 show the angular velocity of the debris for the two and three dimensional cases respectively.
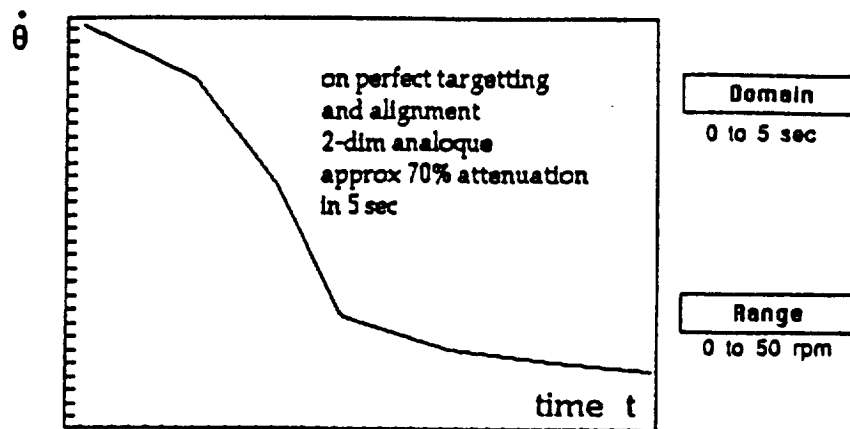

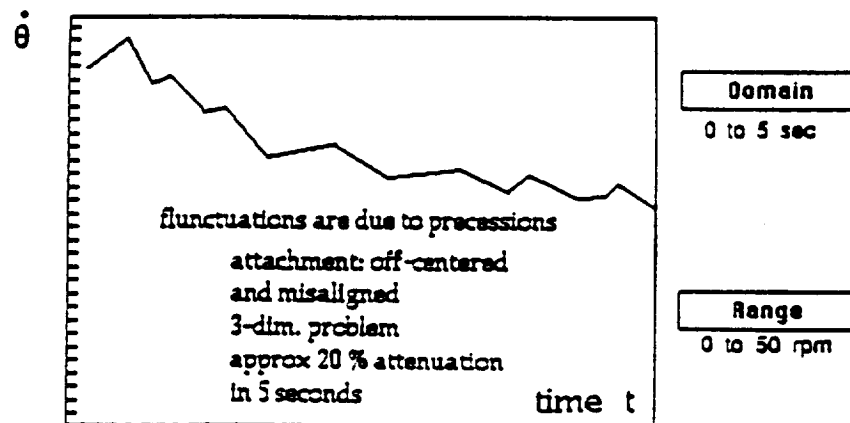Figure 10. 2-D Computer Modeling

Figure 11. 3-D Computer Modeling

The results indicate that the targeting and alignment of our device is essential and therefore a process of determining the center of mass of the debris before operation is essential. The software can provide results once the device is attached on the satellite; however, impact forces caused by the attachment process were not modeled.

To evaluate the model, a final comment on the effects upon impact needs to be made. Provided that no eccentric forces are present, i.e. perfect targeting, any components directed radially from the earth will cause oscillations that are estimated to die out. Moreover, any angular components will result in shifting the orbit but not changing the orbit altitude. Thus, the effects on the debris will be mostly translational and will not greatly affect the attenuation process.

E)   Attachment

Since the purpose of this project was to test processes for attenuation the issue of attaching the mechanism to the satellite was not initially addressed. However, it was felt that developing a method of attachment was necessary to complete the subject of attenuating the rotational motion of orbital debris.

Several ideas were considered. Wrapping something around the satellite (similar to lassoing) was discarded because it could not be guaranteed that there would be a perfectly clear path all the way around every satellite due to auxiliary objects such as antennas. Grabbing the satellite was not felt to be practical because the skin of the satellite is very flimsy (since its only purpose is to shield the inside from solar radiation and small particles) and could not sustain very large forces and moments.

The conceptual design of the device that was chose to build was much like an umbrella. The device would pierce through the skin of the satellite and once inside open up, much like an umbrella, to prevent the device from slipping back out.

As can be seen in Figure 13, a motor turns a threaded rod and the collar with the shorter links attached begins to move. Once the collar contacts the back-plate the collar no longer moves along the threaded rod and the shorter links then pull the larger links until both are at right angles to the threaded rod. The mechanism would have worked with only the longer rods; however, the design chosen minimizes the load that each link has to take and increases the mechanical advantage of each link, thereby requiring less energy.
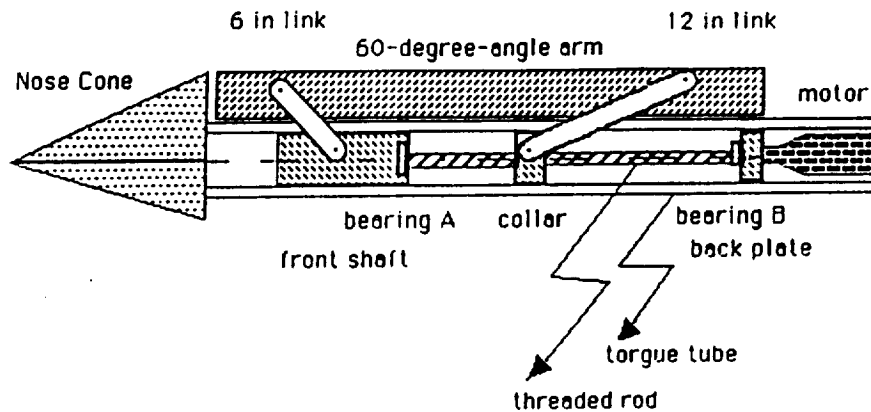
13

Figure 12. Attachment Device

The motor to drive the threaded screw would be a D.C. motor. The batteries would be charged prior to usage utilizing the power source available to ASPOD.

F) Conclusion

The overall purpose of our part of the project was to research and design a mechanism that would slow or attenuate the rotation of a satellite. The solution found would involve launching a geared-bar mechanism to the piece of debris. The tip would pierce the skin and six links would then open up to keep the device in place. The flywheel would then be disconnected from its locked position and allowed to rotate out. This would transfer the rotational energy from the satellite to a more manageable form in the flywheel. This method was proven to work through experimentation and mathematical and computer analysis.

DIGITAL CONTROL OF PLACEMENT ARM

The ASPOD design incorporates a solar-powered metal cutter to facilitate dead satellite processing in a cost effective manner. In order to position debris at the focal point it is necessary that the ASPOD be equipped with robotic arms. The arm function is to hold and move material to be cut in the focal plane of the solar concentrator. After this initial developments stage the gathering arm was controlled with a variable speed on/off control panel. In order to automate the arm and to better simulate its operation in space, a hardware/software controller was designed. The objective of the digital control was to eliminate the direct human interface initially needed to operate the arm and to replace it with a software interface that would accept commands entered into a PC terminal. The digital control would increase the accuracy of the arms' movements and with the software interface, a program could be developed in order to perform a pick-and-place operation or a more defined cutting operation.

Design Specifications

The robotic arm has five revolute joints as shown in Figure 1 with axes and degrees of joint rotation. The most important component of the whole robot system is the digital control system whose components are: a power supply, voltage regulator, two motion controller boards(from Motion Engineering), five motor drivers, five optical encoders, five dc motors, and an IBM PC. Two of the hardware parts - the power supply and the motor driver - required custom design and fabrication. These components were constructed by members of the team.
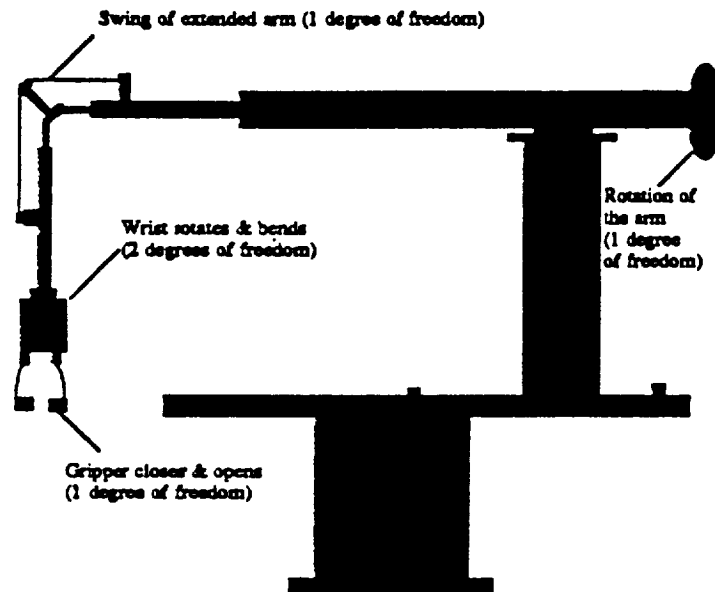

Figure 1. Robotic arm showing degrees of freedom at joints

The hardware needed to build the power supply included a transformer, a bridge and two capacitors to produce a dual output of +25V/-25V with a smooth signal (resembling dc voltage). The +25 V was also connected to a voltage regulator to produce +5 V for the optical encoder. Figure 2 shows the circuit design for both the power supply and the voltage regulator.

Five individual motor drivers (channels) were built within the motor driver. Each driver consisted of a high voltage operational amplifier to amplify the input voltage from motion controller boards, transistors, capacitors and resistors (see Figure 3). The motor driver receives a voltage from the motion controller board between -10V/+10V. The operational amplifier amplifies the voltage at values of +20 to -20V. The transistor amplifies the current and then sends a voltage to drive the DC motors at each joint of the arm.
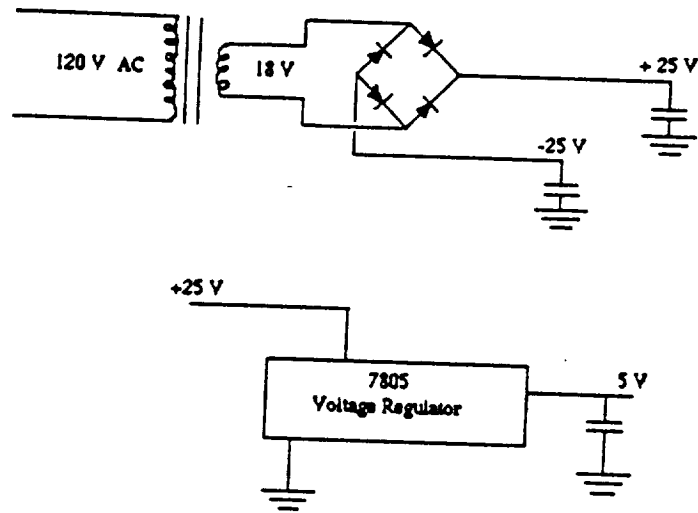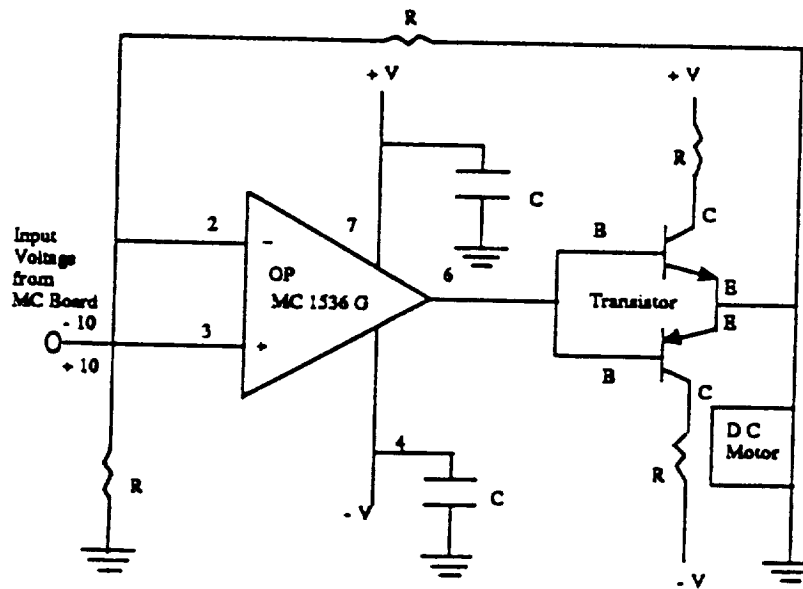
Figure 2. Power supply and Voltage regulator

Figure 3. Circuit design of motor driver

The optical encoders (HEDS-5600) are used to provide accurate motion detection. It provides high performance, optical incremental encoder which emphasize high reliability and

16

resolution, low cost and easy to assemble. The optical encoders were attached at the points of rotation to measure the angle of rotation at each joint. The optical encoders required a rigid mount and modification to the shaft at each joint. Their operational description is located in the Hewlett-Packard specification sheets in appendix. F.

Two motion controller (MC) boards control the five DC motors on the arm. The MC-400 is able to control four motors while MC-200 can control two motors. The two MC boards are connected to the computer and wired to the motor drivers. Included in the package with the controller boards were two types of software: the "Stand Alone Program" aids in the installation and testing of the optical encoders and the MC boards; the "Utility Subroutine and Program" aid in the development of a customer-written program. The software can be written in either "C" or "BASIC". The MC controller boards were accompanied by a user guide to assist in installation and operation. The block diagram for the control system is shown on the next page in Figure 4.
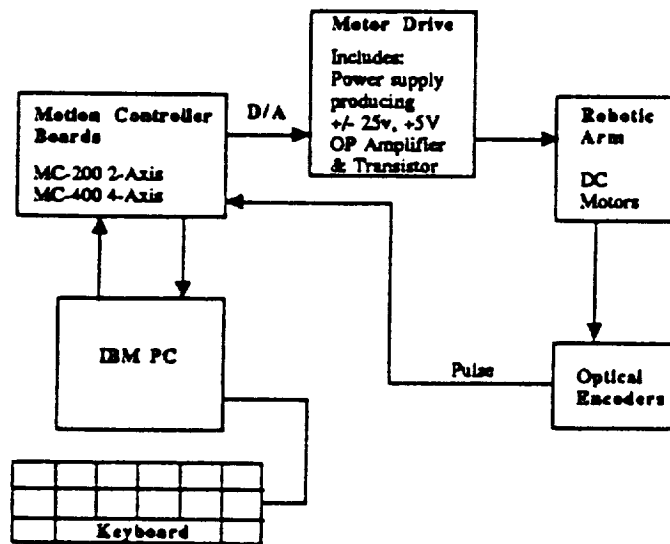
Figure 4. General block diagram for Robotic Arm Control System

The decision was made to use these MC boards over other possible choices because the controller cards were designed around the HCTL-1000 general purpose Motion Control IC. The HCTL-1000 has the capacity to handle all encoder input decoding, phase commutation for steppers and brushless servo motors, digital filtering of the control signal, and generation of analog or pulse-width-modulated motor command signals. It continually performs intensive tasks of digital motion control, therefore freeing the PC for other planning tasks. The HCTL-1000 operation is controlled by a bank of 64 internal registers which in turn, can be accessed

17

by mapping within the PC memory. There is no need for interrupt handling during operation. Refer to appendix. G for design characteristics of the HCTL-1000

To develop the control system, the robotic arm is viewed as a continuous time-varying system. The Laplace transform technique is utilized to simplify the analysis. The block diagram in Figure 5 depicts the feedback closed loop system of the robotic arm control. The digital controller is IBM computer, while the DAC is a digital-to-analog converter, and the ADC is an analog-to-digital converter. The amplifier is the motor driver circuit used to convert the low level analog torque signal u(t) to a voltage v(t) , which directly activates the joint motors. Since the joints are dc motors, the generated torque is proportional to the armature current. Therefore, the amplifier in Figure 5 is an analog subsystem regulating the current through variations in the applied armature voltage. The ADC block detects the position(encoders) and the speed(tachometers) of the joint motors and converts them into a form recognized by the digital controller. Thus, the sensors here represent an encoded disk (optical encoder) of the type analog-to-digital converter.
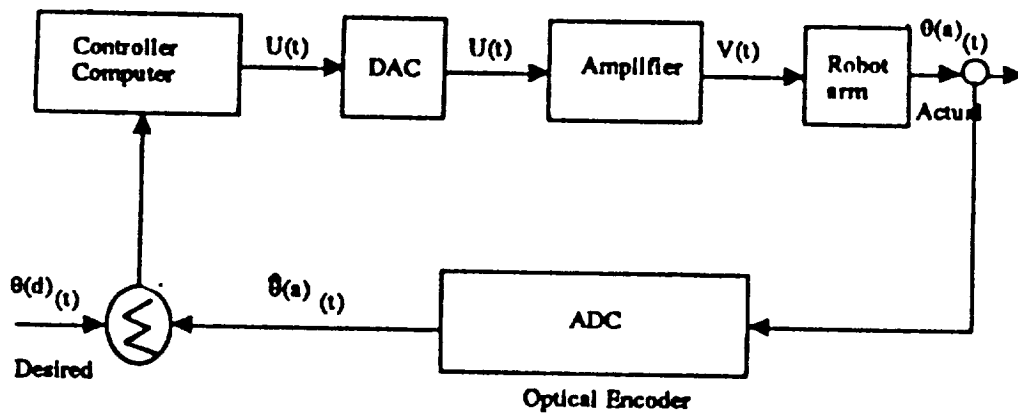
Figure 5. Feedback closed loop system of digital control

The status of the project at this point is that we have control of four of the five motors on the arm. A program was written in "C" which can demonstrate a predetermined movement of the arm and its return. Since the initial (zero) position sensors are not installed, the arm can only be controlled using the joint coordinates. Two sample programs were developed for this purpose. One uses the voltage to control the joints. It reads and records the guadrature

18

counts from the optical encoders. The second program uses the trapezoidal profile position control in an interactive mode. It has been modified to execute a sequence of point - to - point positions in the specified envelope. A copy of both programs is in appendix H. The user at this point may move all joints simultaneously or move one joint at a time to a predefined position. This requires only one keystroke to the keyboard.

Future plan

The future plan of the software project is to move the arm with all five degrees of freedom integrating in a "pick-and-place" fashion. The arm will also be able to be moved to any predetermined position in the physical envelope of the apparatus (i.e move anywhere defined in polar(r,q) coordinates). Future work involves some hardware and software amplifications. For the hardware, some position sensors need to be installed for the initial (zero) position and instal an optical encoder at the wrist. For the software aspect, The relationship between the inverse kinematics of the robot arm and the trajectory planning needs studied in more depth. Integration of the second arm must also be achieved. Components of this integration include state-of-the-art Artificial Intelligence and decentralized control algorithms. Additional considerations for the software portion include both error checking and recovery Software which must be designed with the focal cutting point in mind as well as an initial (zero) position. All of the above points must be intrinsic to the computer software each time the machine is booted up or loaded. The future work of the project will take place in the succeeding semesters by other design teams.

MANIPULATOR ARM

The ASPOD spacecraft will need two robotic arms to succesfully retrieve and process a piece of orbital debris. This year the task was taken to design and fabricate a new robotic arm. This arm was to be designed with the specific ASPOD mission in mind, and have the flexibility necessary for the handling of large pieces of debris.

LIMITATIONS

There will be no subsequent contact with the orbiter once it has been launched, therefore it must be reliable. The arm must have a hand capable of grabbing most space debris as well as grappling with a larger satellite. Control of the arm must be precise. Vibrations must be minimized as well as slop/backlash within the arm's actuator mechanisms. The design must be adaptable to digital control and the electrical system must run off a 24 volt power supply.

DESIGN (TARGET) SPECIFICATIONS

In the process of generating alternative solutions the solar mirror structure was analyzed to determine the necessary DOF's. By approaching the problem in this manner, we would not have to analyze and build models to treat every design that didn't have any immediate foreseeable problems. The analysis by this method led to a very unique solution.

To start, it was determined that the easiest way to remove the lens from the holding slot was to translate it along an axis contained within the plane of the lens., (see fig.1). We can call this the hand axis from here on to clarify our discussion. Note that we assume the grasping mechanism to be attached to this axis.
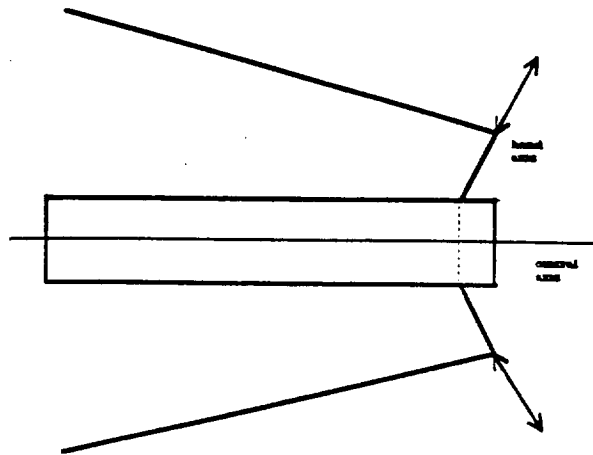
Figure 1. Hand Axis

To reach all three lenses with the hand axis in this orientation with respect to each lens individually, it is necessary to rotate about the central axis of the mirror structure, (see fig.2).
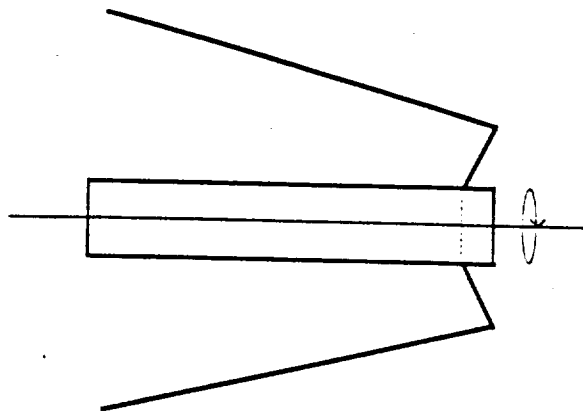
Figure 2. Central Axis Rotation

The next requirement is for the arm to be able to reach the focal point. From figure 3 it can be seen that we need only to translate along an axis parallel to that of the central axis to meet this requirement. Finally, to reach debris located above the mirror structure the mechanism must be able to rotate about an axis perpendicular to the plane created by both the hand and central axis .
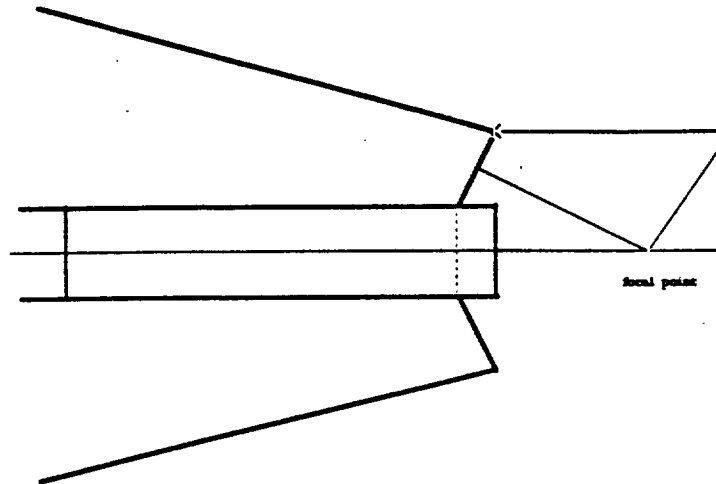

Figure 3. Focal Point Within Reach

With these three DOF's we have a work area with roughly the shape of a cylinder with half spheres at the ends. Adding more DOF's in the form of joints or extensions would be redundant at this point. The adding of redundancies may decrease the difficulty of specific tasks. For example, in the case where an obstruction prevents the arm from directly reaching an object, it may be necessary to have another joint in the arm to essentially reach around the obstruction.

It is important to note that none of the DOF's required by the hand to perform properly have been considered here. The reason is that the DOF's discussed so far are for location and orientation of the hands, i.e.- getting the hand to the desired locations ; whereas, the DOF's required by the hand are for orientation of the hand to receive the object. Those DOF's will be discussed in the subproblems involving the hand.

Using the three fundamental DOF's, the configuration in figure 4 was proposed. Also, the design in figure 8 shows the arm with several redundancies. Note that the ring was used to accomplish the rotation about the central axis so that no part of the arm would be prone to moving through the focal point (see fig. 4&5).
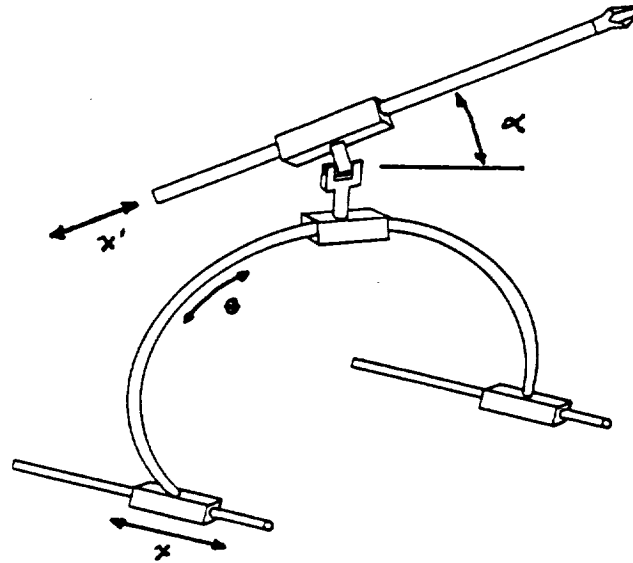
Figure 4. Final Design
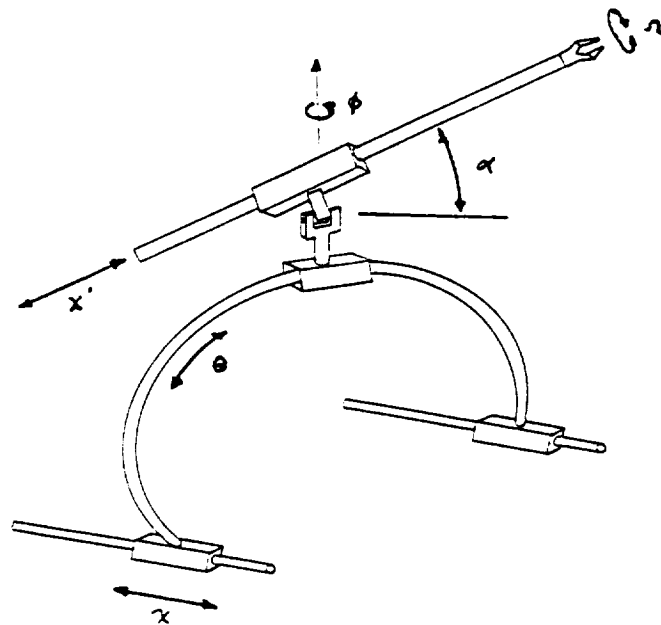
FINAL DESIGN

Figure 5. Final Design

Polar Drive Mechanism

The purpose of the axial tracks is to translate the entire robotic arm structure along the body of the collector (see appendix I.1). This is accomplished through the motor driven screws shown in fig. I.2. The motors have an output of 100 oz-in. at 30 rpm per motor. This velocity will cause the polar track assembly to move at a rate of 4 in./min. The reason for keeping the velocity low is to prevent unwanted oscillations in the system. The power screws are regular 0.5 inch and 13 threads per inch.

The main load of the polar tracks is taken up by the bearings inside the pillow blocks (see fig. I.3). The bearings are 0.75 inch linear bearings. Two linear bearings were used to prevent horizontal motion. The bearings ride on 60 case hardened steel rods. This material was chosen because of its great stiffness capabilities and availability. Along side the bearings, inside the pillow blocks, there are two couplings. The reason for using two is also to prevent horizontal deflection and to maximize the contact area between the pillow blocks and the driver screws.

The connection between the pillow blocks and the polar track is done through the flat plates that are welded to the polar track and the pillow blocks. The flat plates are bolted together.

The tracks are supported at the ends (see fig.I.4). They were manufactured out of aluminum stock.

The circular track allows the arm to rotate about the focal point allowing the arm to align itself in a normal sense to the lens axis. The circular track allows the arm to access the mirror/lens structure without interference. A wide-base channel section (5 X 1.75 inch cross section) provides the necessary contact points to mount the arm and yields a "chamber" of space essential to the drive mechanism (see appendix J.1). The channel material is 5052 aluminum and initially weighed 24 lbs. The weight was reduced to approximately 19 lbs. by drilling thirty 2.5 inch diameter holes along the web and are evenly spaced 3.5 inches apart center to center. The holes did not weaken the track but did slightly deform it. The track's inside diameter was reduced by approximately 0.5 inches and is not a problem.

The arm is mounted onto the arm-platform (see fig. J.2) which contacts the channel track at six points; four on the outside and two on the inside. The rollers are Killian bearings which provide normal and lateral stability. The four outside bearings have been modified to prevent derailing. A washer has been pressed against the lip of the bearing. Two pairs of springs are incorporated in the design of the platform. One pair clamps the inside rollers to the platform providing normal stability, and the other pair ensures lateral contact of the bearings to the track. The springs are necessary to account for track irregularities.

The drive mechanism is shown in appendix J.3. It is simply a dual chain/sprocket drive. Power is transferred through a 50:1 worm gear reducer. The motor ordered was found to be faulty. It was rated at 10,000 rpm, 9 oz-in. torque. It was to operate at shaft conditions of 500 rpm, 180 oz-in. This would give more than the needed torque of 500 oz-in. Testing showed motor output was nowhere near these specs. so it was necessary to use a motor that was found and worked. No characteristics are known about the motor. Testing of the circular track drive mechanism showed that operation

23

performance was adequate for loads of 15 to 20 lbs. Figure () shows theoretical curves for required motor power consumption . Theta refers to the angular position of the drive mechanism.

Elbow Joint

The elbow joint provides one degree of freedom which enables objects to be moved in or out of the focal point. It also supports access radially outward from the polar track providing access to objects which lie outside the ASPOD's framework. The elbow consists of two major components (Fig. K1).

The first piece holds the motor, worm and braces the 5/16" shaft with a 7/8" OD roller bearing press fit at either side. The selected motor is shown below as motor #1. The worm is steel, single tooth and 32 pitch. The shaft is held in place with snap ring.

The second major part of the elbow joint has a 32 pitch 100 tooth worm wheel pressed into it. The worm wheel mates the worm on the first part when placed on the shaft. The shaft has a flat milled across it and is fixed to the worm wheel with a 5-40 set screw. The set screw is 2" long so it not only holds the shaft but also fixes the wheel to the second piece.

Both parts of the elbow have a 1" long hollow male fitting which is placed into a 1.5" OD .0649" thick pipe. All structural parts are made of aluminum, all fasteners are steel.

Motor Rotor Assembly:

The motor rotor assembly is a gearbox which holds the arm above the polar track and allows the arm to rotate a full 360^0 (Fig. L2). This provides access to objects in front, behind or to either side of the ASPOD. The gearbox consists of two 9" x 4" plates separated 2.5" by four spacers (Fig. L3). The motor drives a 24 pitch 100 tooth worm wheel which is held on the end of a shaft end of the shaft/endcap with 5-40 set screw. The motor selected for the gearbox is identified as motor #1. The motor is held at the precise height and angle with the motor mount (Fig. L4).

The shaft/endcap is machined to have a 3/8" shaft on one end and a 1/2" long hollow male fitting on the other. It protrudes through the top of the gearbox so that the 1.5" pipe which holds the elbow joint can be attached (Fig. L2). The part of the endcap which joins the shaft was threaded with 9/32" -18 threads/in. The shaft fits through a bearing and is held by a 9/32" nut. The bearing is held in place with a machined cap. The cap was machined to have a snug fit with the bearing circumference and have a 1/1000" interference fit between the bearing and top plate. The cap is fastened to the plate with four 6/32" bolts.

Motor Selection:

The following motors were selected on their torque and speed. The exact weight was unknown but a rough estimate considering their size was also considered. The motors needed to have this great amount of torque as our initial estimates of the arm weight were too low. These motors will allow the arm to retain its original design capabilities of lifting a 2 lb plate at an extension of 33 in.

Motor#	Quantity	Torque (oz-in)	Speed (RPM)
1	2	100	375
2	1	25	1000
3	3	100	75
4	2	75	30

Grasping Mechanism

The requirements of the grasping mechanism are to be able to grab a thin flat plate ranging in thickness from 0.125 to 0.75 inches, to grasp a cylinder with a diameter ranging from 0.125 to 4.000 inches, and to grasp a sphere with a diameter equal to that of the cylinder. Other general requirements for the mechanism are that the weight be minimal, the ratio of the clamping to the actuator force be maximized, and that the force ratio be as nearly constant throughout the range of motion of the mechanism as is possible.

For the design that was developed and built to meet the requirements the ratio of the clamping force to the actuator force is 0.25 and is nearly constant throughout the clamping range. The ratio was determined by constructing a static force vector diagram on each design at intervals in their range of motion. There was a trade off between the increased ratio and smaller size. In appendix M, figures 1-3 show the selected design in its fully extended, closed and intermediate positions. From figure four of appendix M it can be seen that the force ratio would increase if the distance between the two sets of four bar linkages was increased. This design was chosen over five others because of its higher clamping force ratio, its smaller size, and its simplicity.

Figure five and six of appendix M show the dimensions for both the base and grip respectively. The holes shown in those two drawings have a 0.251 inch diameter to allow for a slip fit around a 0.250 ground pin. Figure seven shows the dimensions for the two different links and push- rod. Table one on page eight of appendix M shows the parts list for the prototype .

The robotic arm must have translation along the axis of the arm and rotation about the circular track to provide access to the focal point of the orbiter.

Harmonic Vibrations

Vibrations of any space structure creates special problems. The payload must be deployed, be able to precisely grab objects and not suffer damage trying to capture satellites due to fatigue.

The space shuttle has a natural harmonic frequency of 32 Hz which prevents it from carrying a payload with a corresponding harmonic frequency less than or equal to 32 Hz. Such a payload ($\geq$ 32 Hz) would certainly cause resonant vibrations of increasing amplitude. Damage to the shuttle resulting from resonance would be likely since it takes several hours to deploy any payload and the shuttle would be subject to the resonant vibrations until deployment since there is no damping in space.

If the robotic arm is to grasp an object, the exact position of the manipulator must be known. Low frequency vibrations tend to have greater amplitude and the end of the arm could move more than an inch. Use of space-rated composite materials (higher structural stiffness) would help to alleviate this problem.

If the amplitude of harmonic vibrations is too high, the robotic arm will experience high stresses. These stresses will cause fatigue damage if aluminum is the primary construction material the arm. This is especially dangerous since space structures usually have little or no factor of safety. Composites have better fatiguing properties and should be used in all high stress areas.

Conclusion

This years research team designed and constructed the primary grappling arm. The arm has the ability to maneuver large and bulky objects into the focus of the frenel lense solar cutting device without obstructing the beam. A secondary function of the arm is to be able to repair or replace any of the frenel lenses if they are damaged. Both of these goals are met with the ASPOD robotic arm.

Most of the design specifications have been met. The arm can grasp a variety of objects from round balls to flat plates. It can be adapted to computer control by future design teams. All motors operate at 24 Volts (some are rated slightly higher but this presents no problem). The arm appears able to replace frenel lenses and repair the mirror array.However, the arm is not light weight in fact it is so overweight that the Polar Arc is in distress. The arm isn't reliable enough to operate for months of years without service.

Replacement of some aluminum parts with graphite composites would greatly increase the performance of the robotic arm. Not only will weight be drastically reduced but problems due to the low harmonics (4 to 10 Hz depending on its position) of the arm will be improved.

REFERENCES

1. Discover, December, 1988, p 22.

2. GEO, March, 1989, p 154.

3. Danish Science, December, 1988, p 46.

4. Smithsonian, December, 1988.

5. Arizona Daily Star, February 21, 1987.

6. Tucson Citizen, February 27, 1987.

7. Arizona Republic, August 14, 1988.

8. Tucson Citizen, September 23, 1988.

9. American Way, May 15, 1989.

10. Artificial Space Debris, Johnson, Nicholas L., Orbit Book Company, Malabar, Florida, 1987.

11. ibid

12. ibid

13. ibid

14. "Debris Danger Zone", Natural History, November, 1987.

15. "Hypervelocity Impact", NASA Activities, April-May, 1987.

APPENDIX A

STABILITY OF A DEFORMABLE GYRO.

* BECAUSE OF INTERNAL FRICTION (ENERGY DISSIPATION), THE KINETIC ENERGY OF A ROTATING GYRO CAN ONLY DECREASE WITH TIME.

∴ STABLE ATTITUDE IS THE ONE FOR WHICH THE KINETIC ENERGY IS THE SMALLEST POSSIBLE, FOR A GIVEN ANGULAR MOMENTUM, WHICH REMAINS CONSTANT.

FOR A RIGID BODY,

$$I = \begin{bmatrix} A & 0 & 0 \\ 0 & B & 0 \\ 0 & 0 & C \end{bmatrix} \quad (PRINCIPAL\ AXIS)$$

INITIALLY, LET

$$\underset{\sim}{\omega} = [e_x \ e_y \ e_z] \begin{bmatrix} \omega_{0x} \\ \omega_{0y} \\ \omega_{0z} \end{bmatrix}$$

∴

$$\underset{\sim}{H_0} = [e_x \ e_y \ e_z] \begin{bmatrix} A\omega_{0x} \\ B\omega_{0y} \\ C\omega_{0z} \end{bmatrix}$$

$$|\underset{\sim}{H_0}| = \sqrt{A^2\omega_{0x}^2 + B^2\omega_{0y}^2 + C^2\omega_{0z}^2}$$

AND

$$T_0 = \frac{1}{2}(A\omega_{0x}^2 + B\omega_{0y}^2 + C\omega_{0z}^2)$$

NOW, FOR $t > t_0$ THE GYRO BECOMES NON-RIGID

∴

$$I = \begin{bmatrix} A & I_{xy} & I_{xz} \\ I_{xy} & B & I_{yz} \\ I_{xz} & I_{yz} & C \end{bmatrix} \qquad WHERE\ I_{xy}, I_{yz}, I_{xz} \ll A,B,C$$

ALSO, ASSUME THE INERTIA PRODUCTS ARE HARMONIC FUNCTIONS OF TIME AND THEY REPRESENT OSCILLATORY DISTORTIONS DURING WHICH ENERGY IS DISSIPATED DUE TO INTERNAL DAMPING.

LET THE FINAL CONDITION $(t = t_f)$ BE

$$\underset{\sim}{\omega_f} = [e_x \ e_y \ e_z] \begin{bmatrix} 0 \\ 0 \\ \vdots \end{bmatrix}$$

WITH

$$\underline{H}_f = [e_x \ c_y \ e_z] \begin{bmatrix} 0 \\ 0 \\ c\omega_f \end{bmatrix}$$

SINCE DURING TRANSITION FROM STATE 0 TO STATE f N/O EXTERNAL TORQUS HAS ACTED ON THE GYRO,

$$\underline{H}_f = \underline{H}_0$$

$$\therefore \quad \omega_f = \sqrt{\frac{A^2}{C^2}\omega_{0_x}^2 + \frac{B^2}{C^2}\omega_{0_y}^2 + \omega_{0_z}^2}$$

AND

$$T_f = \frac{1}{2}C\omega_f^2 .$$

OR $$T_f = \frac{1}{2}\left\{ \frac{A^2}{C}\omega_{0_x}^2 + \frac{B^2}{C}\omega_{0_y}^2 + C\omega_{0_z}^2 \right\}$$

THE KINETIC ENERGY ASSUMES THE SMALLEST POSSIBLE MAGNITUDE IF AND ONLY IF

$$C > B \ , \quad C > A$$

* AT THIS POINT, THE GYRO HAS ASSUMED RIGIDITY.

FROM RIGID BODY CRITERIA WE KNOW THAT A GYRO IS UNSTABLE IF C IS THE INTERMEDIATE INERTIA MOMENT. THUS, ONLY PURE ROTATION ABOUT THE AXIS WITH THE LARGEST INERTIA MOMENT IS STABLE FOR A DISSIPATIVE, REAL, SOLID GYRO

∴ STABLE FOR ROTATION ABOUT AXIS WITH LARGEST INERTIA MOMENT.

APPENDIX B

Rough Calculations

Moment of Inertia and Energy of Debris

$$I_{solid \atop cylinder} = \frac{1}{2}MR^2 = \frac{1}{2} \cdot (2000 kg) \cdot 3^2 m^2 = 9000 \, kg \, m^2$$

$$\omega = \frac{40 \, rev}{min} = \frac{40 \cdot 2\pi}{60 \, sec} \approx 4.2 \, s^{-1}$$

$$L = I\omega = (9 \times 10^3 \, kg \, m^2) \cdot 4.2 \, s^{-1} \approx 38 \times 10^3 \, kg \, m^2 \, s^{-1}$$

$$E_{rot} = \frac{1}{2}I\omega^2 =$$

$$= \frac{1}{2}(9 \times 10^3 \, kg \, m^2)(4.2 \, s^{-1})^2 \approx \boxed{80 \, k \, Joules}$$

Upper limit on time the ASPOD can wait

$$\overline{T} \approx 1 \, week \approx 605 \times 10^3 \, sec$$

$$Power \; \overline{P} = \frac{Energy \; E_{rot}}{Time \; \overline{T}} = \underline{0.13 \, W}$$

For $\overline{T} \approx 1 \, day$, $\overline{P} \approx \underline{1.0 \, W}$

$\overline{T} \approx 1 \, hour$, $\overline{P} = \underline{24 \, W}$

debris – spring system analysis

Equation of Motion (rotating about $\perp$ axis)

$$\int_0^\theta T \cdot d\theta = \int_{\omega_0}^\omega I\omega \, d\omega = \int dE_{potential} \qquad (eq. *)$$

Actually $T = T(\theta)$

Assuming that $T = $ constant equation $*$
becomes:

$$\boxed{T\theta = \frac{1}{2} I \left(\omega^2 - \omega_0^2\right)}$$

Spring Characteristics
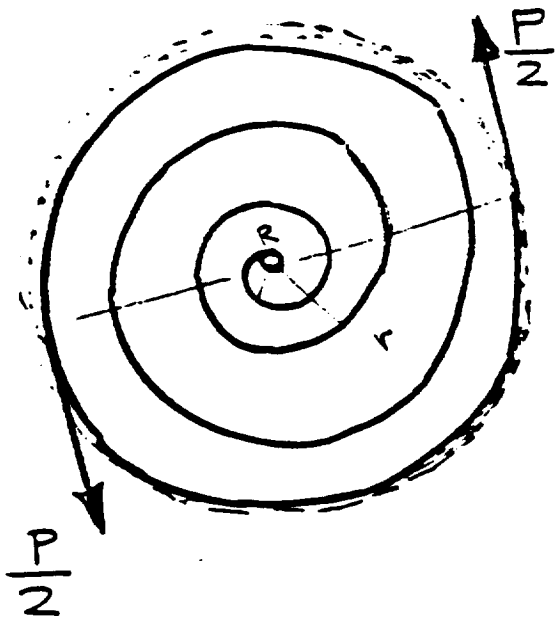
$$T = \frac{P}{2} \cdot 2r = Pr$$
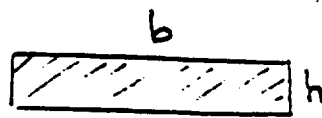
$$I_A = \frac{1}{12}bh^3$$

Take $b = 30\,cm = 0.3\,m$

and $h = 2\,mm = 2\times10^{-3}\,m$ $\Big\}$ $\underline{I_A \approx 2\times10^{-10}\,m^4}$

spring characteristics

$$P = \frac{bh^2 S_s}{6rk} \quad \text{or} \quad T = \frac{bh^2 S_s}{6k}$$

$$\text{where} \quad k = \frac{3c-1}{3c-3} \quad \& \quad c = \frac{2R}{h}$$

Let $R \sim 4cm \Rightarrow c \sim 40$

$$k \sim 1$$

Using steel 4340 Q&T $\boxed{\begin{array}{l} S_y = 1590 \text{ MPa} \\ E = 190 \text{ GPa} \end{array}}$

$$T = \frac{(0.3m)(2 \times 10^{-3}m)^2}{6} \ 1.59 \times 10^9 \ \frac{N}{m^2}$$

$$= 0.32 \cdot 10^3 = \underline{320 \ N \cdot m}$$

Now $f = r\theta = \frac{P\ell r^2}{EI}$ and $\theta = \frac{P\ell r}{EI_A} = \frac{T\ell}{EI_A}$

$$\Rightarrow \quad \theta_{allow} = \frac{320 \ N \cdot m \cdot \ell}{190 \cdot 10^9 \ \frac{N}{m^2} \cdot 2 \times 10^{-10} m^4} = 8.42 \ \ell \ \Longleftarrow$$

radians $\qquad\qquad\qquad\qquad\qquad\qquad\qquad$ meters

$$E_{POTENTIAL} = \int T d\theta = T \cdot \theta$$

$$\theta_{needed} = \frac{80 kJ}{320 \, N \cdot m} \sim 250 \, rad \sim 40 \, revolutions$$

Assume a factor of safety of $\frac{1}{2}$ in θ :

$$\Rightarrow \theta_{needed} = \frac{1}{2} \theta_{allow}$$

Now using $\theta_{allow} = 8.42 \frac{\ell}{meters}$ radians

a spring with total "coiled" length $\ell = 10m$ is required. This will require an outer diameter of about 1 m.

Assuming $\alpha = const.$ (rate of change of $\omega = const$) we obtain $t = \frac{\omega}{\alpha} \sim 126 \, sec \sim 2 \, min$ for the time needed to attenuate.

Notes ① the losses in the ratchet were neglected for the time being

② the alternative of coupling several coiled springs together still needs to be investigat

APPENDIX C

FLYWHEEL RETRACTED

REV	SEC	DELTA	RPM
1	1.10	1.10	54.47
2	3.46	2.36	47.70
3	7.25	3.79	41.97
4	12.52	5.27	40.42
5	19.55	7.03	34.13
6	28.45	8.90	32.13
7	39.55	11.10	27.23
8	53.12	13.57	24.30
9	69.45	16.32	21.82
10	88.90	19.45	19.15
11	111.86	22.96	17.10
12	138.98	27.12	14.44
13	171.09	32.12	12.00
14	209.53	38.44	9.49
15	256.81	47.28	6.78

FLYWHEEL EXTENDED

REV	SEC	DELTA	RPM
1	1.21	1.21	49.55
2	3.68	2.47	47.70
3	7.52	3.84	43.89
4	12.89	5.38	38.98
5	19.91	7.02	36.40
6	28.75	8.84	33.10
7	39.57	10.82	30.24
8	52.48	12.91	28.76
9	67.70	15.22	25.95
10	85.43	17.73	23.85
11	106.02	20.59	20.98
12	129.70	23.68	19.44
13	156.79	27.09	17.61
14	187.70	30.91	15.71
15	223.00	35.30	13.64
16	263.30	40.30	12.00
17	309.71	46.41	9.83
18	363.70	53.98	7.92
19	428.67	64.98	5.46

FLYWHEEL OPERATING

REV	SEC	DELTA	RPM
1	1.66	1.66	36.23
2	3.46	1.80	33.25
3	5.45	1.98	30.24
4	7.75	2.30	26.03
5	10.33	2.58	23.27
6	13.57	3.24	18.51
7	17.64	4.07	14.74
8	22.20	4.56	13.15
9	27.36	5.16	11.64
10	33.35	5.99	10.01
11	40.27	6.92	8.67
12	48.57	8.30	7.23
13	59.38	10.80	5.55
14	77.56	18.19	3.30

APPENDIX D

GEAR-BAR MECHANISM
ANALYSIS

The kinematic constraints are obtained from the center of mass coordinates:

$$0 = -My + m(A-y) + \mu(x-y) \implies y(M+m+\mu) = m\alpha + \mu$$

$$0 = M\beta - m(b-\beta) + \mu\beta \implies \beta(M+m+\mu) = mb$$

Furthermore: $\dot{x}(t) = \rho\dot{\varphi}(t) \to \dot{x}(t) = x_0 + \rho\varphi(t)$

(Note: $(\bar{x}, \bar{y})_{system} = (0,0)$ i.e our frame of

reference is attached to the center of mass

of the overall system.

Upon requiring $\mu, m \ll M$ the above equations

reduce to :

$$\boxed{yM = m\alpha + \mu x} - (1)$$

$$\boxed{\beta M = mb} - (2)$$

(Note: $\mu, m \ll M$ means $M+m+\mu \to M$
however:
products of μ & m with relevant
distances are kept.)

Calculation of moments of inertia of components (debris, gear, bar) about (0,0)

$$I_{do} = \frac{1}{2}MR_s^2 + M(y^2 + \beta^2) = \left(\frac{1}{2}MR_s^2 + M\beta^2\right) + My^2$$

$$I_{go} = \frac{1}{2}\mu R_w^2 + \mu\left[(x-y)^2 + (b-\beta)^2\right] =$$

$$= \left[\frac{1}{2}\mu R_w^2 + \mu(b-\beta)^2\right] + \mu(x-y)^2$$

$$I_{bo} = \frac{mL^2}{12} + m\left[(a-y)^2 + (b-\beta)^2\right] = \left[\frac{mL^2}{12} + m(b-\beta)^2\right] + m(a-y$$

$$\sum I = I_{do} + I_{go} + I_{bo} =$$

$$= I_{do\,const} + I_{do}'(t) + I_{go\,const} + I_{go}'(t) +$$

$$+ I_{bo\,const.} + I_{bo}'(t)$$

$$\boxed{\sum I = I_{CONST} + My^2 + \mu(x-y)^2 + m(a-y)^2}$$

Since $y = y(t)$ & $x = x(t)$ $a = const.$

$$\sum I = \sum I(t) = \sum I(\varphi)$$

Now from the the <u>dynamical equations</u> obtained from the Lagrangian $\boxed{\mathcal{L} = \frac{1}{2}\Sigma I(\varphi)\dot{\theta}^2 + \frac{1}{2} I_{\varphi}\dot{\varphi}^2}$

$*$ $\Sigma I(\varphi)\,\dot{\theta} = \Sigma I(\varphi=0)\cdot\dot{\theta}_o$
(Conservation of Angular Momentum)

$**$ $\frac{1}{2}R_w^2 \dfrac{(M+m+H)^2}{Mp^2}\,\ddot{y} = \dot{\theta}^2\Big\{ My - m(\alpha-y) + \dfrac{M+m}{M}\big[(M+m)y - m\cdot$

Upon requiring $m \ll M$ the above equations reduce to $\Sigma I(\varphi)\cdot\dot{\theta} = \Sigma I(\varphi=0)\,\dot{\theta}_o$

& $\dfrac{\cancel{M^2}y^2}{\cancel{M}}\dot{\theta} = \dfrac{\cancel{M^2}y_o^2\,\dot{\theta}_o}{\cancel{M}}$ explicitly

i.e $\boxed{\dot{\theta} = \dfrac{y_o^2\,\dot{\theta}_o}{y^2} = \dfrac{const.}{y^2}}$ $-(3)$

& $My\dot{\theta}^2\Big\{\cancel{M} + \dfrac{M}{M}\Big\} = \dfrac{R_w^2 M^2}{2Mp^2}\,\ddot{y}$

i.e $\dfrac{\cancel{M^2}y\dot{\theta}^2}{\cancel{M}} = \dfrac{R_w^2\cancel{M^2}}{2\cancel{M}p^2}\,\ddot{y}$ $\Rightarrow$ $\boxed{\ddot{y} = \Big(\dfrac{p}{R_w}\Big)^2 2y\dot{\theta}^2}\, (4)$

From (3) solving for $\dot\theta$ and substituting $y = y($ ᵍ

we get:

$$\dot\theta = \frac{y_o^2 \dot\theta_o}{\left(y_o + \frac{\mu P}{M} q\right)^2} \qquad (5$$

Substituting this into (4) we obtain $\ddot y = \ddot y(y)$

which becomes:

$$\ddot y\, y^3 = 2\left(\frac{P}{R_w}\right)^2 y_o^4\, \dot\theta_o^2 = const. \qquad (\,$$

where $\ddot y = \dfrac{d^2 y}{dt^2}$

Equation (6) is a non-linear ODE of the 2nd order. It can be solved analytically for the velocity $\dot y$ as $\dot y = \dot y(y)$ but not as $\dot y = \dot y(t)$

Replacing $\ddot y$ with $\dot y \dfrac{d\dot y}{dy}$ renders the O.D.E separable & upon integrating we obtain:

$$\dot y = \sqrt{12}\left(\frac{P}{R_w}\right)\dot\theta_o \sqrt{1 - \left(\frac{y_o}{y}\right)^4}$$

Using the kinematic constraint $\dot y = \dfrac{\mu \dot x}{M} = \dfrac{\mu P \dot q}{M}$
also
we can obtain the functional relation $\dot x = \dot x(t)$.

<u>To obtain</u> a means of comparison as well e

evaluation of the design (full-scale, using the

<u>actual constraints</u> of $\dot{\theta}_0 = 50 \text{ rpm} \approx 5.24 \text{ rad/sec}$

and $M = 2000 \text{ kg}$, $R_S = 3 \text{ m}$)

and designing with $R_g = 0.5 \text{ m}$, $\rho = 0.05 \text{ m}$

$\mu = 20 \text{ kg}$ & $m = 40 \text{ kg}$

and $L_{bar} = 3 \text{ m}$, from $\dot{\theta} = \dfrac{5.24 \text{ rad/sec}}{(1 + 0.01 \, \varphi)^2}$

we obtain:

$$\left. \dot{\theta} \right|_{\substack{\varphi = 8 \text{ revolutions} \\ = 50 \text{ rad.}}} \sim 50\% \, \dot{\theta}_0$$

(<u>Note</u>: usable bar length is only $L = 2.5 \text{ m}$,

that is the total length minus the radius of

the gear-wheel.)

still

Something that ∧ needs to be investigated ase

the actual $\dot{\varphi}$ values attainable (i.e angular

speed of gear as it rolls out) and the effec

high $\dot{\varphi}$ will have —if any— on the rack.

APPENDIX E

SPACE DEBRIS DATA SET

part/01,ground
marker/0101

part/02, mass=2000, cm=0201, qg=0,0,0, reuler=0,0,0
,ip=7000,7000,9000,0,0,0
,wz=5
marker/0201
marker/020211,qp=0, 3.0,0, reuler=0,90D,90D
marker/028,qp=0,1,0
marker/029,qp=0,-1,0
marker/0210,qp=1,0,0
marker/0211,qp=-1,0,0
marker/020212,qp=0, 3.5,0, reuler=0,90D,90D
marker/02022, qp=0, 3, -0.2
marker/0203, qp=0, 0, 0
marker/02041, qp=0, 0, 2.0
marker/02051, qp=0, 3, 2.0
marker/02061, qp=0, 5, 0
marker/02071, qp=0, 7, 0
marker/02042, qp=0, 0, -2.0
marker/02052, qp=0, 3, -2.0
marker/02062, qp=0, 5, -0.2
marker/02072, qp=0, 7, -0.2

part/03, mass=20,   cm=0301, qg=-0.03,3.5,0, reuler=0,0,0
,ip=3,3,5.0,0,0,0
marker/0301
marker/03011, qp= 0,   0,   0, reuler= 90D,180D,90D
marker/0302, qp= 0.03, 0,   0, reuler=-90D,0,0
marker/0303, qp= 0, -0.03, 0,
marker/0304, qp=-0.03, 0,   0
marker/0305, qp= 0,   0.03, 0
marker/031, qp=0.5,0,0
marker/032, qp=0,-5,0
marker/033, qp=-0.5,0,0
marker/034, qp=0,5,0

part/04, mass=2, cm=04011, qg=0,3.5,0, reuler=0,0,0
,ip=0.5,0.5,0.5, 0,0,0
marker/04011
marker/04012,qp=0,0,0, reuler=0,90D,90D
marker/0402, qp=-0.03,0,0, reuler=90D,180D,0
marker/0403, qp=0,0,0, reuler=0,90D,90D

!   joint/99,i=0302,j=020212
!   ,rackpin, pd=0.03

gear/1, joints=24,34, cv=0403
joint/24, i=020212, j=04012, translational
joint/34, i=03011, j=0402, revolute

```
request/01, displacement, i=0201, j=0101
request/02, velocity    , i=0201, j=0101
request/03, acceleration, i=0201, j=0101

request/04, displacement, i=0301, j=0201
request/05, velocity    , i=0301, j=0201
request/06, acceleration, i=0301, j=0201
```

```
!                     GRAPHICS OUTPUT

graphics/11
,outline=020211,02061,02071,02072,02062,02022,020211

graphics/22
,cylinder
,cm=0203, radius=3
,length=2, sides=40, seg=40

graphics/33
,cylinder
,cm=0203, radius=3
,length=-2, sides=40, seg=40

graphics/44
,cylinder
,cm=0301, radius=0.5
,length=0.2, sides=40, seg=40

graphics/55
,outline=0302,0304,0302

graphics/66
,outline=0303,0305,0303

graphics/77
,outline=028,029,028

graphics/88
,outline=0210,0211,0210

graphics/99
,outline=031,033,031

graphics/111
,outline=032,034,032


output/grsave,reqsave

results/formatted
,comment=space debris attenuation data

debug/ dump,verbose,dof,topology

end
```

SPACE DEBRIS DATA SET

!   PARTS AND THEIR MARKERS

part/01,ground
marker/0101

part/02, mass=2000, cm=0201, qg=0,0,0, reuler=0,0,0
,ip=7000,7000,9000,0,0,0
,wz=-5
marker/0201
marker/020211,qp=0, 3.0,0, reuler=0,90D,90D
marker/028,   qp=0,1,0
marker/029,   qp=0,-1,0
marker/0210,   qp=1,0,0
marker/0211,   qp=-1,0,0
marker/020212,qp=0, 3.5,0, reuler=0,90D,90D
marker/02022, qp=0, 3, -0.2
marker/0203,   qp=0, 0, 0
marker/02041, qp=0, 0, 2.0
marker/02051, qp=0, 3, 2.0
marker/02061, qp=0, 5, 0
marker/02071, qp=0, 7, 0
marker/02042, qp=0, 0, -2.0
marker/02052, qp=0, 3, -2.0
marker/02062, qp=0, 5, -0.2
marker/02072, qp=0, 7, -0.2

part/03, mass=20,   cm=0301, qg=-0.03,3.5,0, reuler=0,0,0
,ip=3,3,5.0,0,0,0
marker/0301
marker/03011, qp= 0,   0,   0, reuler= 90D,180D,90D
marker/0302, qp= 0.03, 0,   0, reuler=-90D,0,0
marker/0303, qp= 0, -0.03, 0,
marker/0304, qp=-0.03, 0,   0
marker/0305, qp= 0,   0.03, 0

part/04, mass=2, cm=04011, qg=0,3.5,0, reuler=0,0,0
,ip=5,5,5, 0,0,0
marker/04011
marker/04012,qp=0,0,0, reuler=0,90D,90D
marker/0402, qp=-0.03,0,0, reuler=90D,180D,0
marker/0403, qp=0,0,0, reuler=0,90D,90D

!   CONSTRAINTS

!   joint/99,i=0302,j=020212
!   ,rackpin, pd=0.03

gear/1, joints=24,34, cv=0403
joint/24, i=020212, j=04012, translational
joint/34, i=03011, j=0402, revolute

!   REQUEST OUTPUT

request/01, displacement, i=0201, j=0101
request/02, velocity   , i=0201, j=0201

```
request/04, displacement, i=0301, j=0201
request/05, velocity    , i=0301, j=0201
request/06, acceleration, i=0301, j=0201




!                          GRAPHICS OUTPUT

graphics/11
,outline=020211,02061,02071,02072,02062,02022,020211

graphics/22
,cylinder
,cm=0203, radius=3
,length=2, sides=40, seg=40

graphics/33
,cylinder
,cm=0203, radius=3
,length=-2, sides=40, seg=40

graphics/44
,cylinder
,cm=0301, radius=0.5
,length=0.2, sides=40, seg=40

graphics/55
,outline=0302,0304,0302

graphics/66
,outline=0303,0305,0303

graphics/77
,outline=028,029,028

graphics/88
,outline=0210,0211,0210




output/grsave,reqsave

results/formatted
,comment=space debris attenuation data

debug/ dump,verbose,dof,topology

end
```

SPACE DEBRIS DATA SET   .

!   PARTS AND THEIR MARKERS

part/01,ground
marker/0101

part/02, mass=2000, cm=0201, qg=0,0,0, reuler=0,0,0
,ip=6900,7100,8900,100,100,100
,wz=5
marker/0201
marker/020211,qp=0, 3.0,0, reuler=0,90D,90D
marker/028,qp=0,1,0
marker/029,qp=0,-1,0
marker/0210,qp=1,0,0
marker/0211,qp=-1,0,0
marker/020212,qp=0, 3.5,0, reuler=0,90D,90D
marker/02022, qp=0, 3, -0.2
marker/0203, qp=0, 0, 0
marker/02041, qp=0, 0, 2.0
marker/02051, qp=0, 3, 2.0
marker/02061, qp=0, 5, 0
marker/02071, qp=0, 7, 0
marker/02042, qp=0, 0, -2.0
marker/02052, qp=0, 3, -2.0
marker/02062, qp=0, 5, -0.2
marker/02072, qp=0, 7, -0.2

part/03, mass=20,   cm=0301, qg=-0.03,3.5,0, reuler=0,0,0
,ip=3,3,5.0,0,0,0
marker/0301
marker/03011, qp= 0,   0,   0, reuler= 90D,180D,90D
marker/0302, qp= 0.03, 0,   0, reuler=-90D,0,0
marker/0303, qp= 0, -0.03, 0,
marker/0304, qp=-0.03, 0,   0
marker/0305, qp= 0,   0.03, 0

part/04, mass=2, cm=04011, qg=0,3.5,0, reuler=0,0,0
,ip=0.5,0.5,0.5,0,0,0
marker/04011
marker/04012,qp=0,0,0, reuler=0,90D,90D
marker/0402, qp=-0.03,0,0, reuler=90D,180D,0
marker/0403, qp=0,0,0, reuler=0,90D,90D

!   CONSTRAINTS

!   joint/99,i=0302,j=020212
!   ,rackpin, pd=0.03

gear/1, joints=24,34, cv=0403
joint/24, i=020212, j=04012, translational
joint/34, i=03011, j=0402, revolute

!   REQUEST OUTPUT

request/01, displacement, i=0201, j=0101
request/02, velocity   , i=0201, j=0101
request/03, acceleration, i=0201, j=0101

```
request/04, displacement, i=0301, j=0201
request/05, velocity    , i=0301, j=0201
request/06, acceleration, i=0301, j=0201




!                      GRAPHICS OUTPUT

graphics/11
,outline=020211,02061,02071,02072,02062,02022,020211

graphics/22
,cylinder
,cm=0203, radius=3
,length=2, sides=40, seg=40

graphics/33
,cylinder
,cm=0203, radius=3
,length=-2, sides=40, seg=40

graphics/44
,cylinder
,cm=0301, radius=0.5
,length=0.2, sides=40, seg=40

graphics/55
,outline=0302,0304,0302

graphics/66
,outline=0303,0305,0303

graphics/77
,outline=028,029,028

graphics/88
,outline=0210,0211,0210




output/grsave,reqsave

results/formatted
,comment=space debris attenuation data

debug/ dump,verbose,dof,topology

end
```

SPACE DEBRIS DATA SET

PARTS AND THEIR MARKERS

part/01,ground
marker/0101

part/02, mass=2000, cm=0201, qg=0,0,0, reuler=0,0,0
,ip=7000,7000,9000,0,0,0
,wz=5
marker/0201
marker/020211,qp=0, 3.0,0, reuler=0,90D,90D
marker/028,   qp=0,1,0
marker/029,   qp=0,-1,0
marker/0210,   qp=1,0,0
marker/0211,   qp=-1,0,0
marker/020212,qp=0, 3.5,0, reuler=0,90D,90D
marker/02022, qp=0, 3, -0.2
marker/0203,   qp=0, 0,   0
marker/02041, qp=0, 0,   2.0
marker/02051, qp=0, 3,   2.0
marker/02061, qp=0, 5,   0
marker/02071, qp=0, 7,   0
marker/02042, qp=0, 0, -2.0
marker/02052, qp=0, 3, -2.0
marker/02062, qp=0, 5, -0.2
marker/02072, qp=0, 7, -0.2

part/03, mass=80,   cm=0301, qg=-0.03,3.5,0, reuler=0,0,0
,ip=12,12,15,0,0,0
marker/0301
marker/03011, qp= 0,   0,   0, reuler= 90D,180D,90D
marker/0302, qp= 0.03, 0,   0, reuler=-90D,0,0
marker/0303, qp= 0, -0.03, 0,
marker/0304, qp=-0.03, 0,   0
marker/0305, qp= 0,   0.03, 0

part/04, mass=2, cm=04011, qg=0,3.5,0, reuler=0,0,0
,ip=0.5,0.5,0.5, 0,0,0
marker/04011
marker/04012,qp=0,0,0, reuler=0,90D,90D
marker/0402, qp=-0.03,0,0, reuler=90D,180D,0
marker/0403, qp=0,0,0, reuler=0,90D,90D

CONSTRAINTS

joint/99,i=0302,j=020212
,rackpin, pd=0.03

gear/1, joints=24,34, cv=0403
joint/24, i=020212, j=04012, translational
joint/34, i=03011, j=0402, revolute

REQUEST OUTPUT

request/01, displacement, i=0201, j=0101
request/02, velocity   , i=0201, j=0101
request/03, acceleration, i=0201, j=0101

```
request/04, displacement, i=0301, j=0201
request/05, velocity    , i=0301, j=0201
request/06, acceleration, i=0301, j=0201



!                       GRAPHICS OUTPUT

graphics/11
,outline=020211,02061,02071,02072,02062,02022,020211

graphics/22
,cylinder
,cm=0203, radius=3
,length=2, sides=40, seg=40

graphics/33
,cylinder
,cm=0203, radius=3
,length=-2, sides=40, seg=40

graphics/44
,cylinder
,cm=0301, radius=0.5
,length=0.2, sides=40, seg=40

graphics/55
,outline=0302,0304,0302

graphics/66
,outline=0303,0305,0303

graphics/77
,outline=028,029,028

graphics/88
,outline=0210,0211,0210



output/grsave,reqsave

results/formatted
,comment=space debris attenuation data

debug/ dump,verbose,dof,topology

end
```

SPACE DEBRIS DATA SET   .

part/01,ground
marker/0101

part/02, mass=2010, cm=0201, qg=0,0,0, reuler=0,0,0
,ip=7000,7000,9000,0,0,100
,wz=5
marker/0201
marker/020211,qp=0, 3.0,0, reuler=0,90D,90D
marker/028,   qp=0,1,0
marker/029,   qp=0,-1,0
marker/0210, qp=1,0,0
marker/0211, qp=-1,0,0
marker/020212,qp=0, 3.5,0, reuler=0,90D,90D
marker/02022, qp=0, 3, -0.2
marker/0203, qp=0, 0, 0
marker/02041, qp=0, 0, 2.0
marker/02051, qp=0, 3, 2.0
marker/02061, qp=0, 5, 0
marker/02071, qp=0, 7, 0
marker/02042, qp=0, 0, -2.0
marker/02052, qp=0, 3, -2.0
marker/02062, qp=0, 5, -0.2
marker/02072, qp=0, 7, -0.2

part/03, mass=20,   cm=0301, qg=-0.03,3.5,0, reuler=0,0,0
,ip=3,3,5.0,0,0,0
marker/0301
marker/03011, qp= 0,   0,   0, reuler= 90D,180D,90D
marker/0302, qp= 0.03, 0,   0, reuler=-90D,0,0
marker/0303, qp= 0,   -0.03, 0,
marker/0304, qp=-0.03, 0,   0
marker/0305, qp= 0,   0.03, 0

part/04, mass=2, cm=04011, qg=0,3.5,0, reuler=0,0,0
,ip=0.5,0.5,0.5, 0,0,0
marker/04011
marker/04012,qp=0,0,0, reuler=0,90D,90D
marker/0402, qp=-0.03,0,0, reuler=90D,180D,0
marker/0403, qp=0,0,0, reuler=0,90D,90D

!   joint/99,i=0302,j=020212
!   ,rackpin, pd=0.03

gear/1, joints=24,34, cv=0403
joint/24, i=020212, j=04012, translational
joint/34, i=03011, j=0402, revolute

request/01, displacement, i=0201, j=0101
request/02, velocity   , i=0201, j=0101
request/03, acceleration, i=0201, j=0101

```
request/04, displacement, i=0301, j=0201
request/05, velocity    , i=0301, j=0201
request/06, acceleration, i=0301, j=0201




!                         GRAPHICS OUTPUT

graphics/11
,outline=020211,02061,02071,02072,02062,02022,020211

graphics/22
,cylinder
,cm=0203, radius=3
,length=2, sides=40, seg=40

graphics/33
,cylinder
,cm=0203, radius=3
,length=-2, sides=40, seg=40

graphics/44
,cylinder
,cm=0301, radius=0.5
,length=0.2, sides=40, seg=40

graphics/55
,outline=0302,0304,0302

graphics/66
,outline=0303,0305,0303

graphics/77
,outline=028,029,028

graphics/88
,outline=0210,0211,0210



output/grsave,reqsave

results/formatted
,comment=space debris attenuation data

debug/ dump,verbose,dof,topology

end
```

```
10 DIM TIME(2000)
20 CLS:X=1
30 OPEN"c:\123\123.fil\data.prn" FOR OUTPUT AS #1
40 A$=INKEY$:TIME(X)=TIMER:IF A$="" THEN 40
50 PRINT X,TIME(X)-TIME(1),TIME(X)-TIME(X-1),60/(TIME(X)-TIME(X-1))
60 PRINT #1,X,TIME(X)-TIME(1),TIME(X)-TIME(X-1),60/(TIME(X)-TIME(X-1))
70 X=X+1
80 IF A$=CHR$(27) THEN 100
90 GOTO 40
100 CLOSE:SHELL"123"
110 GOTO 20
```

APPENDIX F

Features

- QUICK AND EASY ASSEMBLY
- NO SIGNAL ADJUSTMENT REQUIRED
- LOW COST
- SMALL SIZE
- HIGH PERFORMANCE
- HIGH RESOLUTION
- INSENSITIVE TO RADIAL AND AXIAL PLAY
- -40° C TO 100° C OPERATING TEMPERATURE
- TWO CHANNEL QUADRATURE OUTPUT
- TTL COMPATIBLE OUTPUTS
- SINGLE 5 V SUPPLY

Description

The HEDS-5500 is a high performance, low cost, optical incremental encoder which emphasizes high reliability, high resolution and easy assembly.

The encoder contains a lensed LED light source, an integrated circuit with detectors and output circuitry, and a code wheel which rotates between the emitter and detector IC. The outputs of the encoder are two square waves in quadrature. The collimated light and special photodetector configuration allow for high resolution and excellent encoding performance as well as increased long life reliability.
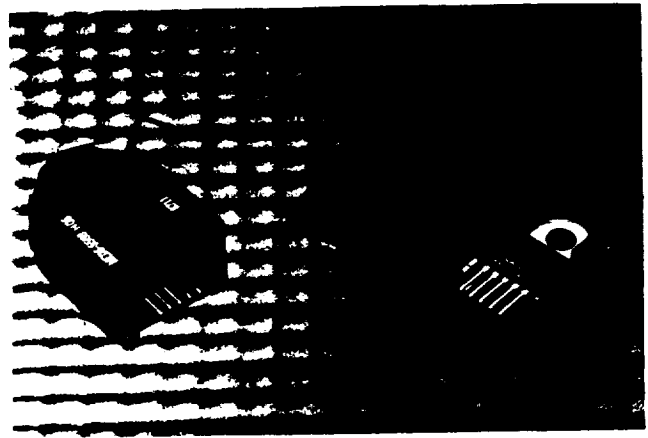
The encoder may be quickly and easily mounted onto a motor. No mechanical or electrical adjustments are required.

The two channel digital outputs and the single 5 V supply input are accessed through 0.025 inch square pins located on 0.1 inch centers.

Applications

The HEDS-5500 provides motion detection at a low cost, making it ideal for high volume applications. Typical applications include printers, plotters, tape drives, positioning tables and automatic handlers.
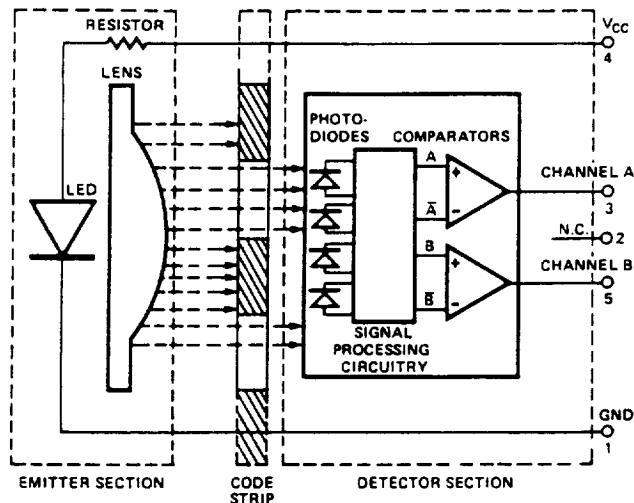
ESD WARNING: NORMAL HANDLING PRECAUTIONS SHOULD BE TAKEN TO AVOID STATIC DISCHARGE.
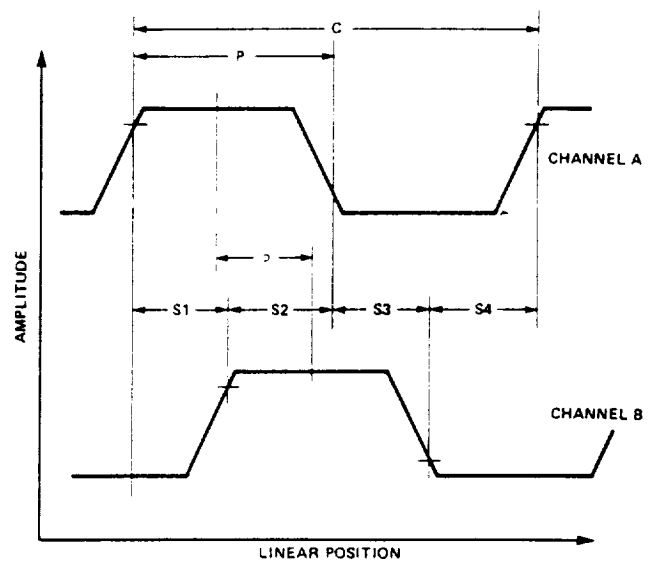
Outline Drawing

Block Diagram

EMITTER SECTION   CODE STRIP   DETECTOR SECTION

Output Waveforms

LINEAR POSITION
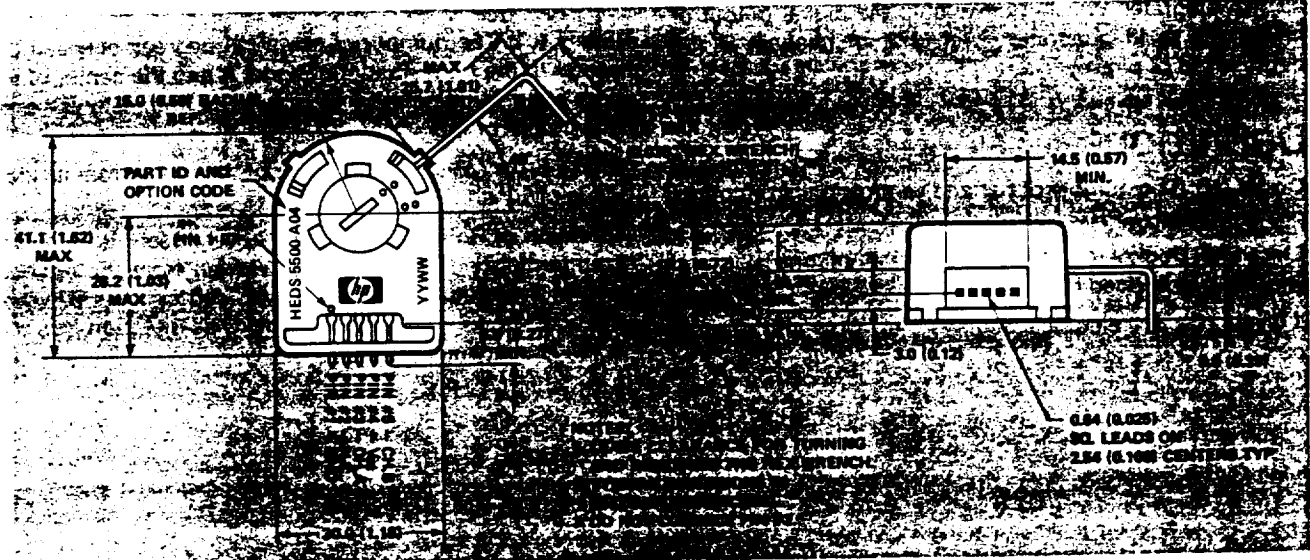
Theory of Operation

The HEDS-5500 translates rotary motion of a shaft into a two channel digital quadrature output.

As seen in the block diagram, the HEDS-5500 encoder contains a single Light Emitting Diode (LED) as its emitter. The light is collimated into a parallel beam by means of a single lens located directly over the LED. Opposite the emitter is an integrated detector circuit. This IC consists of multiple sets of photodetectors and the signal processing circuitry necessary to produce the digital waveforms.

The code wheel rotates between the emitter and detector, causing the light beam to be interrupted by the code wheel's pattern of spaces and bars. The photodiodes which detect these interruptions are arranged in a pattern that corresponds to the radius and design of the code wheel. These detectors are also spaced such that a light period on one pair of detectors corresponds to a dark period on the adjacent pair of detectors. The photodiode outputs are then fed through the signal processing circuitry resulting in A, $\overline{A}$, B and $\overline{B}$. Two comparators receive these signals and produce the final outputs for channels A and B. Due to this integrated phasing technique, the digital output of channel A is in quadrature with that of channel B (90 degrees out of phase).

Definitions

Count (N): The number of bar and window pairs or counts per revolution (CPR) of the code wheel.

Electrical Degree (°e): The dimension of one bar and window pair divided by 360.

1 Cycle (C): 360 electrical degrees (°e), 1 bar and window pair.

1 Shaft Rotation: 360 mechanical degrees. N cycles.

Position Error ($\Delta\theta$): The normalized angular difference between the actual shaft position and its position as indicated by the encoder cycle count.

Cycle Error (ΔC): An indication of cycle uniformity. The difference between an observed shaft angle which gives rise to one electrical cycle, and the nominal angular increment of 1/N of a revolution.

Pulse Width (P): The number of electrical degrees that an output is high during 1 cycle. This value is nominally 180°e or 1/2 cycle.

Pulse Width Error (ΔP): The deviation, in electrical degrees, of the pulse width from its ideal value of 180°e.

State Width (S): The number of electrical degrees between a transition in the output of channel A and the neighboring transition in the output of channel B. There are 4 states per cycle, each nominally 90°e.

State Width Error (ΔS): The deviation, in electrical degrees, of each state width from its ideal value of 90°e.

Phase (ϕ): The number of electrical degrees between the center of the high state of channel A and the center of the high state of channel B. This value is nominally 90°e for quadrature output.

Phase Error ($\Delta\phi$): The deviation of the phase from its ideal value of 90°e.

Direction of Rotation: When the code wheel rotates in the counterclockwise direction (as viewed from the encoder end of the motor), channel A will lead channel B. When the code wheel rotates in the clockwise direction, channel B will lead channel A.

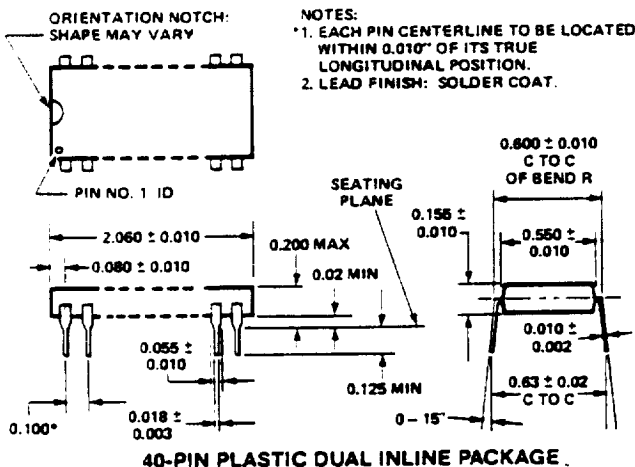# APPENDIX G

![HP Logo] **HEWLETT PACKARD**

GENERAL PURPOSE MOTION CONTROL IC
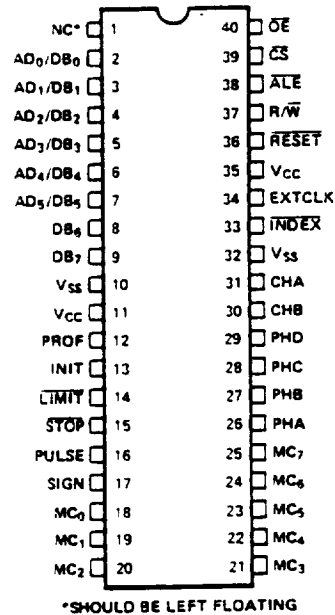
HCTL-1000

Features

- DC, DC BRUSHLESS AND STEPPER MOTOR CONTROL
- POSITION CONTROL
- VELOCITY CONTROL
- PROGRAMMABLE VELOCITY PROFILING
- PROGRAMMABLE DIGITAL FILTER
- PROGRAMMABLE COMMUTATOR
- PROGRAMMABLE PHASE OVERLAP
- PROGRAMMABLE PHASE ADVANCE
- GENERAL 8 BIT PARALLEL I/O PORT
- 8 BIT PARALLEL MOTOR COMMAND PORT
- PWM MOTOR COMMAND PORT
- QUADRATURE DECODER FOR ENCODER SIGNALS
- 24 BIT POSITION COUNTER
- SINGLE 5 V POWER SUPPLY
- TTL COMPATIBLE
- 1 OR 2 MHz CLOCK OPERATION

Package Dimensions

40-PIN PLASTIC DUAL INLINE PACKAGE

NOTES:
*1. EACH PIN CENTERLINE TO BE LOCATED WITHIN 0.010" OF ITS TRUE LONGITUDINAL POSITION.
2. LEAD FINISH: SOLDER COAT.

General Description

The HCTL-1000 is a high performance, general purpose motion control IC fabricated in Hewlett-Packard NMOS technology. It performs all the time-intensive tasks of digital motion control, thereby freeing the host processor for other tasks. The simple programmability of all control 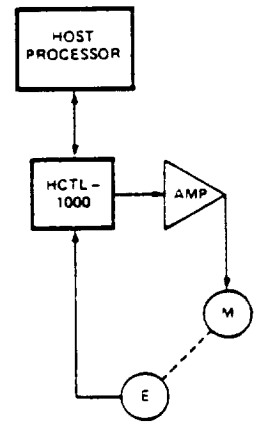parameters provides the user with maximum flexibility and quick design of control systems with a minimum number of components. All that is needed for a complete servo system is a host processor to specify commands, an amplifier and motor with an incremental encoder. No analog compensation or velocity feedback is necessary (see Figure 1).

PINOUT

*SHOULD BE LEFT FLOATING

Figure 1. System Block Diagram

Table of Contents

ESD WARNING: Since this is an NMOS device, normal precautions should be taken to avoid static damage.
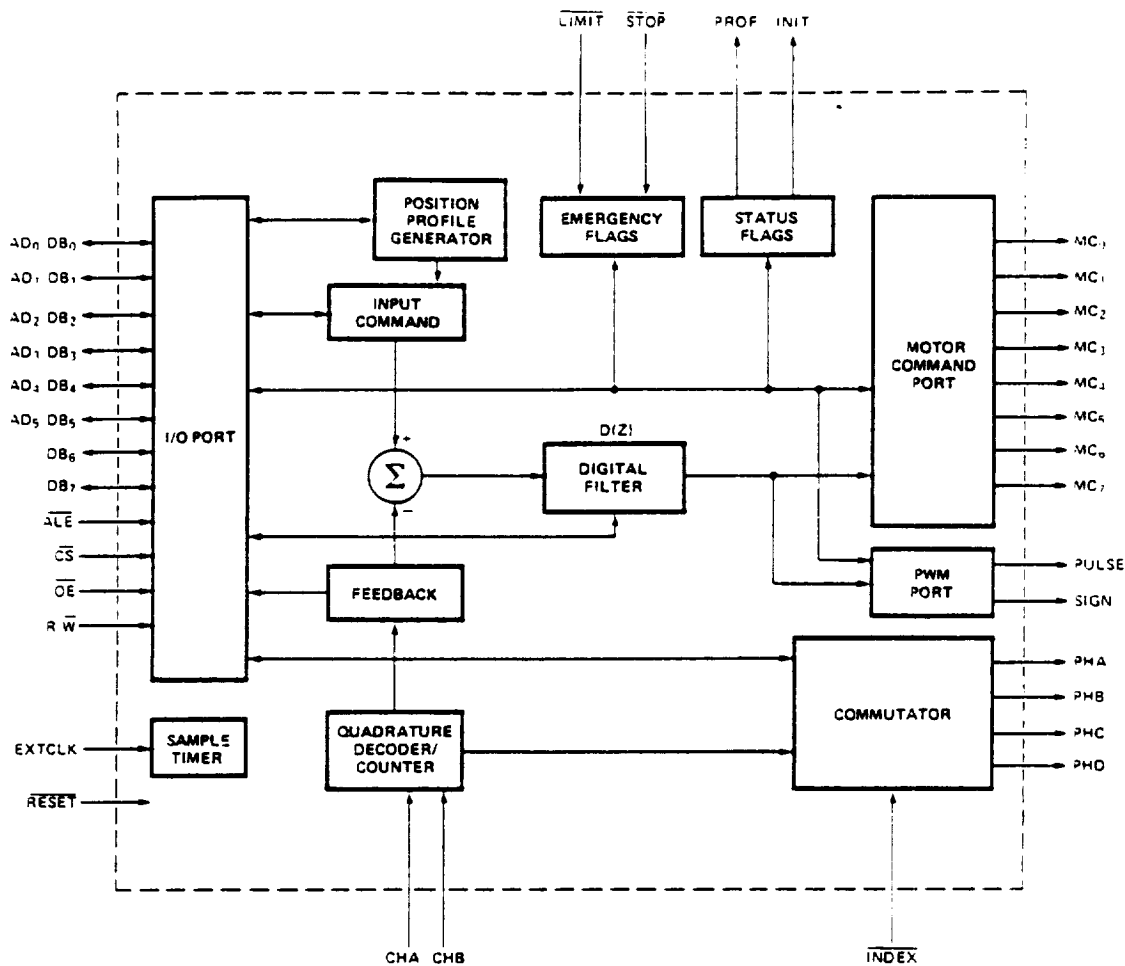
Figure 2. Internal Block Diagram

Introduction

The purpose of this section is to describe the organization of this data sheet. The front page includes the key features of the HCTL-1000, a general description of the part, the mechanical drawing and pin-out, and a Table of Contents. Following this section is the Theory of Operation, which gives the user a brief overview of how the HCTL-1000 operates by describing the internal block diagram shown in Figure 2. The following five sections give the specifications of the HCTL-1000, including Absolute Maximum Ratings, DC Characteristics, AC Characteristics, Timing Diagrams, and Functional Pin Descriptions. The final two sections include the detailed information on how to operate and interface to the HCTL-1000. The How to Operate section discusses the function and address of each software register and describes how to use the four position and velocity control modes and the electronic commutator. The How to Interface section describes how to interface the HCTL-1000 to a microprocessor, an encoder, and an amplifier.

Theory of Operation

The HCTL-1000 is a general purpose motor controller which provides position and velocity control for dc, dc brushless and stepper motors. The internal block diagram of the HCTL-1000 is shown in Figure 2. The HCTL-1000 receives it input commands from a host processor and position feedback from an incremental encoder with quadrature output. An 8-bit directional multiplexed address/data bus interfaces the HCTL-1000 to the host processor. The encoder feedback is decoded into quadrature counts and a 24-bit counter keeps track of position. The HCTL-1000 executes any one of four control algorithms selected by the user. The four control modes are:

- Position Control
- Proportional Velocity Control
- Trapezoidal Profile Control for point to point moves
- Integral Velocity Control with continuous velocity profiling using linear acceleration

The resident Position Profile Generator calculates the necessary profiles for Trapezoidal Profile Control and Integral Velocity Control. The HCTL-1000 compares the desired position (or velocity) to the actual position (or velocity) to compute compensated motor commands using a programmable digital filter D(z). The motor command is externally available at the Motor Command port as an 8-bit byte and at the PWM port as a Pulse Width Modulated (PWM) signal.

The HCTL-1000 has the capability of providing electronic commutation for dc brushless and stepper motors. Using the encoder position information, the motor phases are enabled in the correct sequence. The commutator is fully programmable to encompass most motor encoder combinations. In addition, phase overlap and phase advance can be programmed to improve torque ripple and high speed performance. The HCTL-1000 contains a number of flags including two externally available flags, Profile and Initialization, which allow the user to see or check the status of the controller. It also has two emergency flags, Limit and Stop, which allow operation of the HCTL-1000 to be interrupted under emergency conditions.

The HCTL-1000 controller is a digitally sampled data system. While information from the host processor is accepted asynchronously with respect to the control functions, the motor command is computed on a discrete sample time basis. The sample timer is programmable.

Absolute Maximum Ratings

Operating Temperature .... 0°C to 70°C
Storage Temperature .... -40°C to -125°C
Supply Voltage .... -0.3 V to 7 V
Input Voltage .... -0.3 V to 7 V
Maximum Power Dissipation .... 0.95 W
Maximum Clock Frequency .... 2 MHz

D.C. Characteristics $T_A = 0°C$ to $-70°C$, $V_{CC} = 5 V \pm 5\%$; $V_{SS} = 0 V$

Parameter	Symbol	Min.	Typ.	Max.	Units	Test Conditions
Power Supply	V_{CC}	4.75	5.00	5.25	V	
Supply Current	I_{CC}		80	180	mA	
Input Leakage Current	I_{il}			10	μA	$V_{IN} = 5.25 V$
Tristate Output Leakage Current	I_{loh}			± 10	μA	$V_{OUT} = -0.3$ to 5.25 V
Input Low Voltage	V_{IL}	-0.3		0.8	V	
Input High Voltage	V_{IH}	2.0		V_{CC}	V	
Output Low Voltage	V_{OL}	-0.3		0.4	V	$I_{OL} = 2.2$ mA
Output High Voltage	V_{OH}	2.4		V_{CC}	V	$I_{OH} = -200 \mu A$
Power Dissipation	P_D		400	950	mW	
Input Capacitance	C_{IN}			20	pF	$T_A = 25°C$, f = 1 MHz unmeasured pins returned to ground
Output Capacitance Load	C_{OUT}		100		pF	Same as above

A.C. Electrical Characteristics $T_A = 0°C$ to $70°C$. $V_{CC} = 5\ V \pm 5\%$. Units = nsec

			Clock Frequency			
			2 MHz		1 MHz	
ID#	Signal	Symbol	Min.	Max.	Min.	Max.
1	Clock Period	t_{CPER}	500		1000	
2	Pulse Width, Clock High	t_{CPWH}	230		300	
3	Pulse Width, Clock Low	t_{CPWL}	200		200	
4	Clock Rise and Fall Time	t_{CR}		50		50
5	Input Pulse Width Reset	t_{IRST}	2500		5000	
6	Input Pulse Width Stop, Limit	t_{IP}	600		1100	
7	Input Pulse Width Index, Index	t_{IX}	1600		3100	
8	Input Pulse Width CHA, CHB	t_{IAB}	1600		3100	
9	Delay CHA to CHB Transition	t_{AB}	600		1100	
10	Input Rise/Fall Time CHA, CHB, Index	t_{IABR}		450		900
11	Input Rise/Fall Time Reset, ALE, CS, OE, Stop, Limit	t_{IR}		50		50
12	Input Pulse Width ALE, CS	t_{IPW}	80		80	
13	Delay Time, ALE Fall to CS Fall	t_{AC}	50		50	
14	Delay Time, ALE Rise to CS Rise	t_{CA}	50		50	
15	Address Set Up Time Before ALE Rise	t_{ASR1}	20		20	
16	Address Set Up Time Before CS Fall	t_{ASR}	20		20	
17	Write Data Set Up Time Before CS Rise	t_{DSR}	20		20	
18	Address/Data Hold Time	t_{H}	20		20	
19	Set Up Time, R/W Before CS Rise	t_{WCS}	20		20	
20	Hold Time, R/W After CS Rise	t_{WH}	20		20	
21	Delay Time, Write Cycle, CS Rise to ALE Fall	t_{CSAL}	1700		3400	
22	Delay Time, Read/Write, CS Rise to CS Fall	t_{CSCS}	1500		3000	
23	Write Cycle, ALE Fall to ALE Fall For Next Write	t_{WC}	1830		3530	
24	Delay time, CS Rise to OE Fall	t_{CSOE}	1700		3200	
25	Delay Time, OE Fall to Data Bus Valid	t_{OEDB}	100		100	
26	Delay Time, CS Rise to Data Bus Valid	t_{CSDB}	1800		3300	
27	Input Pulse Width OE	t_{IPWOE}	100		100	
28	Hold Time, Data Held After OE Rise	t_{DOEH}	20		20	
29	Delay Time, Read Cycle, CS Rise to ALE Fall	t_{CSALR}	1820		3320	
30	Read Cycle, ALE Fall to ALE Fall For Next Read	t_{RC}	1950		3450	
31	Output Pulse Width, PROF, INIT, Pulse, Sign, PHA-PHD, MC Port	t_{OF}	500		1000	
32	Output Rise/Fall Time, PROF, INIT, Pulse, Sign PHA-PHD, MC Port	t_{OR}	20	150	20	150
33	Delay Time, Clock Rise to Output Rise	t_{EP}	20	300	20	300
34	Delay Time, CS Rising to MC Port Valid	t_{CSMC}		1600		3200
35	Hold Time, ALE High After CS Rise	t_{ALH}	100		100	
36	Pulse Width, ALE High	t_{ALPWH}	100		100	

APPENDIX H

oasis.ece.arizona.edu:oasis

sample3.c

Thu Jun 7 13:22:55 1990

lw / LaserWriter II NTX

```
lw oasis.ece.arizona.edu:oasis   Job: sample3.c   Date: Thu Jun   7 13:22:55 1990

lw oasis.ece.arizona.edu:oasis   Job: sample3.c   Date: Thu Jun   7 13:22:55 1990

lw oasis.ece.arizona.edu:oasis   Job: sample3.c   Date: Thu Jun   7 13:22:55 1990

lw oasis.ece.arizona.edu:oasis   Job: sample3.c   Date: Thu Jun   7 13:22:55 1990
```

```c
/***************************************************************************/
/*                                                                       */
/*                    M O T I O N   E N G I N E E R I N G                 */
/*                                                                       */
/*          Program Name:  SAMPLE3.C              Date: June 6, 1990     */
/*                                                                       */
/*          Author(s):     Ya-Dung Pan            Revision:  1.0         */
/*                                                                       */
/*                                                                       */
/*          Function:      Sample program uses idle control mode         */
/*                         for voltage control.                          */
/*                                                                       */
/*                                                                       */
/***************************************************************************/
#include        <stdio.h>
#include        <conio.h>
#define MC400
#include         "mc.h"

void border(int, int, int, int, int);
extern void welcome();

main()
{
  int axis;
  int i;
  char input[50];
  long final_pos;
  unsigned char max_vel;
  unsigned int acc;
  int active_axes;
  int running_flag;
  long segment;
  long offset;
  long address;
  long voltage;
  signed char voltage_axis;
  char inchar;
  char input_buff[80];
  char *input_line;
  long encoder[6];

  welcome();
  clrscr();
  printf("This program resets the controllers for 4 axes, then performs an\n");
  printf("idle control mode to move the specified joints using voltage control.\n")

  /* This address needs to be changed for new setup */
     segment = 0xA000L;
     offset = 0x0100L;


  printf("\n");
  printf(" -----------------------------------------------------------------\n")
  printf("|  This program setups the controller board at memory address as    |\n"
  printf("|                  %lx : %lx                                          |\n",
  printf(" -----------------------------------------------------------------\n")


  mc_init(segment, offset);

  for(axis = 0; axis < MAX_AXES; axis++)
    {
      mc_reset(axis);

      mc_set_gain(axis,128);
```

```c
        mc_set_pole(axis,32);
        mc_set_zero(axis,253);

        mc_set_pc(axis,IDLE);
        mc_clr_position(axis);
/*      mc_set_command(axis,0);  */
    }


    getch();
    clrscr();
    border(1,1,80,25,RED);

    window(2,2,44,13);
    border(2,2,44,13,GREEN);

    gotoxy(2,2);
    cprintf("Command formats:\n");
    gotoxy(2,3);
    cprintf("*****************************************\n");
    gotoxy(2,4);
    cprintf("*        Joint #, command (e.g. 1,100)   *\n");
    gotoxy(2,5);
    cprintf("* where command -127 is -10 Volt,        *\n");
    gotoxy(2,6);
    cprintf("*                 0   is   0 Volt,       *\n");
    gotoxy(2,7);
    cprintf("*               127 is  10 Volt,         *\n");
    gotoxy(2,8);
    cprintf("*        joint  0:3     999 for exiting *\n");
    gotoxy(2,9);
    cprintf("*****************************************\n");
    cprintf("\n");

    window(2,13,40,24);
    border(2,13,40,24,GREEN);

    window(41,13,79,24);
    border(41,13,79,24,GREEN);

    axis= 0;
    while (axis != 999)
      { window(2,13,39,24);
        gotoxy(2,2);
        clreol();
        cprintf("Enter command:    ");
        gets(input);
        if (sscanf(input,"%d, %ld", &axis, &voltage) >0 && axis < MAX_AXES

                                        && voltage <= 127 && voltage >= -127)
          {
            gotoxy(2,3);
            cprintf("--> Move joint %d at %.2f V \n\n", axis, voltage*10.0/127.0);
            voltage_axis= voltage + 128;
            mc_set_motor(axis,voltage_axis);

            while (!kbhit())
              { window(41,13,79,24);
                for (i=0; i<MAX_AXES; i++)
                  {
                    encoder[i] = mc_get_position(i);
                    gotoxy(2,i+2);
                    cprintf("encoder position %d : %ld \n", i, encoder[i] );
                  }
              }
          }
```

```c
        else
         {
           gotoxy(2,5);
           cprintf("%c!!! Wrong command, enter again !!!\n",0x007);
         }
      }


}


void border (int startx, int starty, int endx, int endy, int color)
{
   register int i;

   textcolor(color);
   gotoxy(1,1);
   for (i=0; i<=endx-startx; i++)
      putch(0xCD);

   gotoxy(1,endy-starty);
   for (i=0; i<=endx-startx; i++)
   putch(0xCD);

   for (i=2; i<endy-starty; i++)
    { gotoxy(1,i);
      putch(0xBA);
      gotoxy(endx-startx+1, i);
      putch(0xBA);
    }
   gotoxy(1,1);
   putch(0xC9);
   gotoxy(endx-startx+1,1);
   putch(0xBB);
   gotoxy(1,endy-starty);
   putch(0xC8);
   gotoxy(endx-startx+1,endy-starty);
   putch(0xBC);

   textcolor(YELLOW);
  }
```

oasis.ece.arizona.edu:oasis

sample4.c

Thu Jun 7 13:23:58 1990

lw / LaserWriter II NTX

```
lw oasis.ece.arizona.edu:oasis  Job: sample4.c  Date: Thu Jun  7 13:23:58 1990

lw oasis.ece.arizona.edu:oasis  Job: sample4.c  Date: Thu Jun  7 13:23:58 1990

lw oasis.ece.arizona.edu:oasis  Job: sample4.c  Date: Thu Jun  7 13:23:58 1990

lw oasis.ece.arizona.edu:oasis  Job: sample4.c  Date: Thu Jun  7 13:23:58 1990
```

```c
/*******************************************************************/
/*                                                               */
/*                  M O T I O N   E N G I N E E R I N G           */
/*                                                               */
/*        Program Name:  SAMPLE4.C          Date: June 6, 1990   */
/*                                                               */
/*        Author(s):     Ya-Dung Pan        Revision:  2.0       */
/*                                                               */
/*                                                               */
/*        Function:      Sample program uses Trapezoidal Profile */
/*                       Position Control Mode                   */
/*                                                               */
/*                                                               */
/*******************************************************************/
#include         <stdio.h>
#include         <graphics.h>
#include         <conio.h>
#define MC400
#include          "mc.h"
void border(int, int, int, int, int);
extern void welcome();

main()
{
   int axis;
   int i;
   char input[50];
   long final_pos;
   unsigned char max_vel;
   unsigned int acc;
   int active_axes;
   int running_flag;
   long segment;
   long offset;
   long address;
   long voltage;

   char inchar;
   char input_buff[80];
   char *input_line;
   long encoder[6];

   welcome();
   clrscr();
   printf("This program resets the controllers for 4 axes, then performs an\n");
   printf("trapezoidal profile position  control mode to move the specified\n");
   printf("joints. \n");

   /* This address needs to be changed for new setup */
      segment = 0xA000L;
      offset = 0x0100L;


   printf("\n");
   printf(" ----------------------------------------------------------------\n")
   printf("|  This program setups the controller board at memory address as  |\n"
   printf("|                  %lx : %lx                                     |\n",
   printf(" ----------------------------------------------------------------\n")


   mc_init(segment, offset);

   for(axis = 0; axis < MAX_AXES; axis++)
      {
        mc_reset(axis);
```

```c
        mc_set_gain(axis,250);
        mc_set_pole(axis,64);
        mc_set_zero(axis,128);

        mc_set_pc(axis,CONTROL);
        mc_clr_position(axis);
        mc_set_command(axis,0);
    }
        mc_set_gain(3,200);

getch();
clrscr();
border(1,1,80,25,RED);

window(2,2,44,13);
border(2,2,44,13,GREEN);

gotoxy(2,2);
cprintf("Command formats:\n");
gotoxy(2,3);
cprintf("*****************************************\n");
gotoxy(2,4);
cprintf("*         Joint #, command (e.g. 1,200)    *\n");
gotoxy(2,5);
cprintf("* where command -300:300   encoder         *\n");
gotoxy(2,6);
cprintf("*                            pulses        *\n");
gotoxy(2,7);
cprintf("*                                          *\n");
gotoxy(2,8);
cprintf("*         joint    0:3       999 for exiting *\n");
gotoxy(2,9);
cprintf("*****************************************\n");
cprintf("\n");

window(2,13,40,24);
border(2,13,40,24,GREEN);

window(41,13,79,24);
border(41,13,79,24,GREEN);

window(45,2,79,13);
border(45,2,79,13,GREEN);

axis= 0;
while (axis != 999)
  { window(2,13,39,24);
    gotoxy(2,2);

    clreol();
    cprintf("Enter command:    ");
    gets(input);
    if (sscanf(input,"%d, %ld", &axis, &voltage) >0 && axis < MAX_AXES && voltage
      {
        mc_set_final(axis, voltage);
        mc_set_mvel(axis, 100);
        mc_set_accel(axis,10);

        mc_set_flags(axis,TRAP_SET);

        running_flag = 1;
        while (running_flag || !kbhit() )
          { running_flag = 0;
            window(41,13,79,24);
            for (i=0; i<MAX_AXES; i++)
              {
```

```c
                encoder[i] = mc_get_position(i);
                gotoxy(2,i+2);
                cprintf("encoder position %d : %ld \n", i, encoder[i] );
              }
            window(45,2,79,13);
            for (i=0; i<MAX_AXES; i++)
            {
              gotoxy(2,i+2);
              cprintf("command position %d : %ld \n", i, mc_get_command(i) );
            }
            if (mc_get_status(axis) & PROFILE_FLAG) running_flag = 1;
          }
      }
    else
      {
        gotoxy(2,5);
        cprintf("%c!!! Wrong command, enter again !!!\n",0x007);
      }
  }


}


void border (int startx, int starty, int endx, int endy, int color)
{
  register int i;

  textcolor(color);
  gotoxy(1,1);
  for (i=0; i<=endx-startx; i++)
      putch(0xCD);

  gotoxy(1,endy-starty);
  for (i=0; i<=endx-startx; i++)
  putch(0xCD);

  for (i=2; i<endy-starty; i++)
    { gotoxy(1,i);
      putch(0xBA);
      gotoxy(endx-startx+1, i);
      putch(0xBA);
    }
  gotoxy(1,1);
  putch(0xC9);
  gotoxy(endx-startx+1,1);
  putch(0xBB);
  gotoxy(1,endy-starty);
  putch(0xC8);
  gotoxy(endx-startx+1,endy-starty);
  putch(0xBC);

  textcolor(YELLOW);
  }
```

APPENDIX I

Polar Track Final Dimensions

(Dimensions in inches)
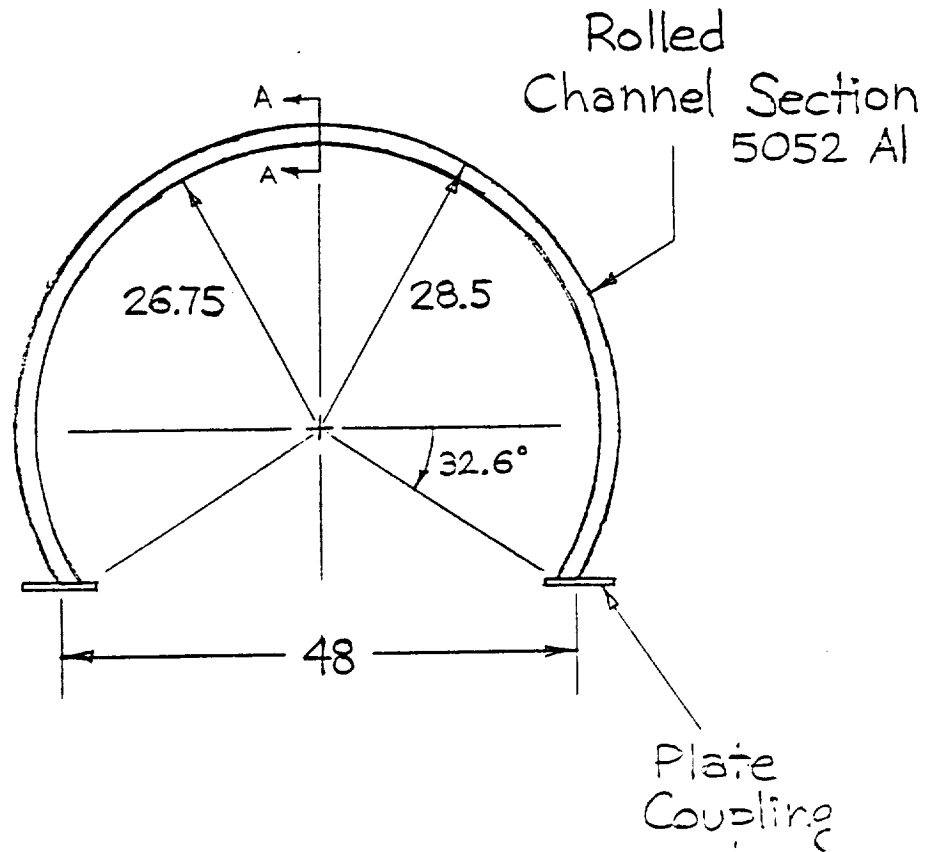
Rolled
Channel Section
5052 Al

A
A

26.75

28.5

32.6°

48

Plate
Coupling

Section A-A:

5052 Aluminum

1.75

0.19

5

C.1

Aluminum Plate

9"

1"

4"

4"

Extension Spring

3/8" Shaft

Killian Bearing (6 Total)

Compressive Spring (2 Total)

ARM PLATFORM

C.2
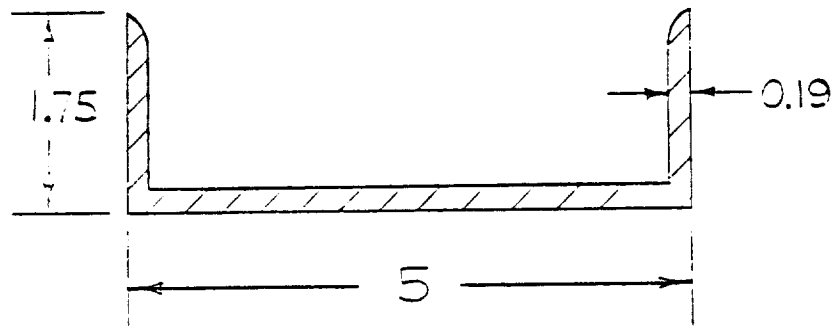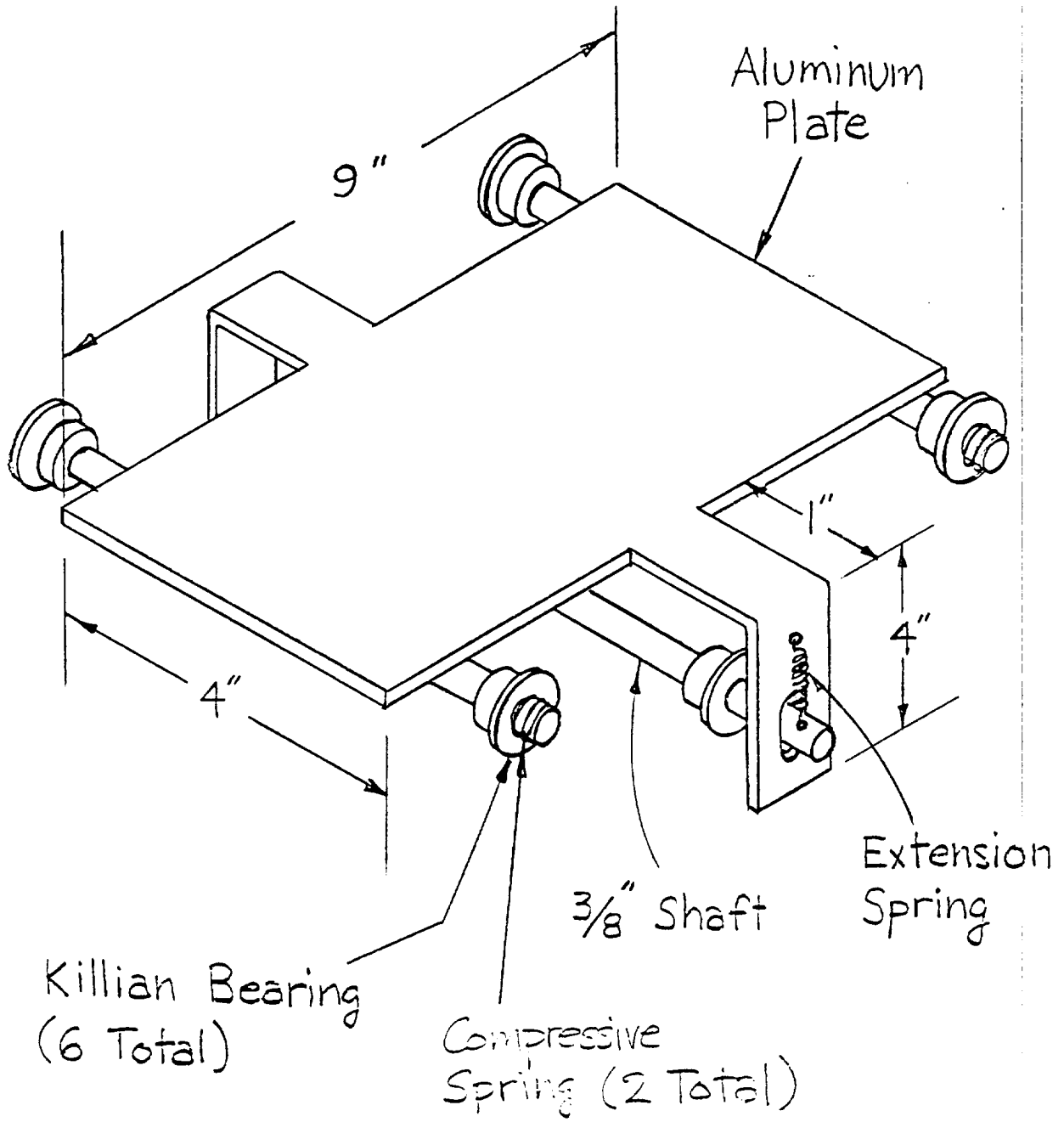
APPENDIX J

DRIVE MECHANISM:

2" Sprocket

DC Motor

Channel Section

Chain ($\frac{1}{4}$" pitch)

Worm Gear Reduction (50:1)

C.3
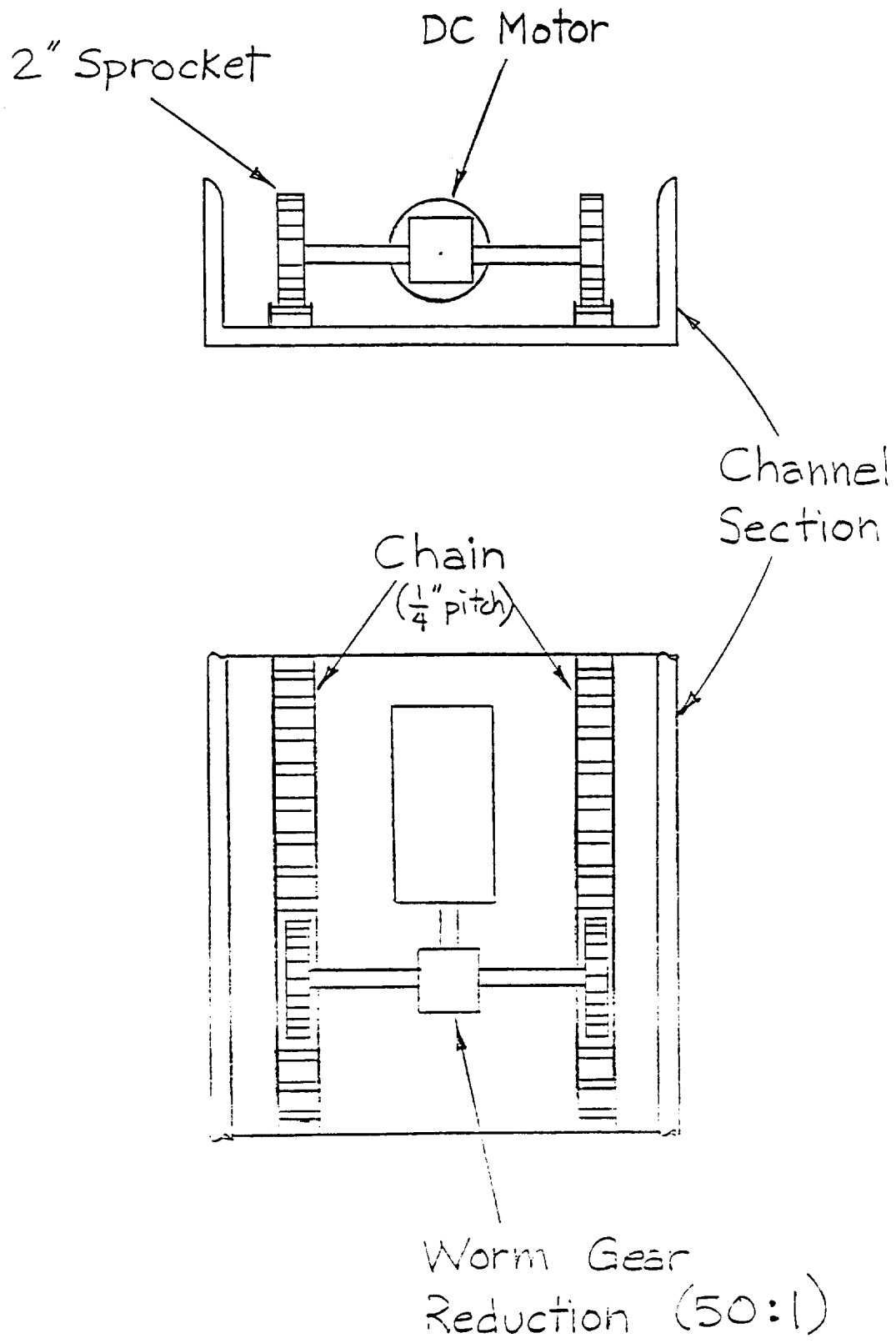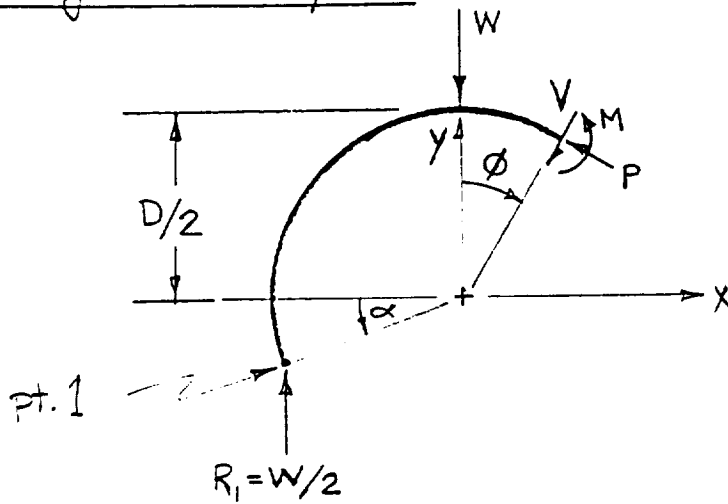
Strength Analysis:

Assume: 1) Load applied statically at top
2) Reaction forces sustain vertical components only.

Basic Equations:

$$\sum F_x = 0 \Rightarrow -V\sin\phi - P\cos\phi = 0$$

$$\sum F_y = 0 \Rightarrow R_1 - W - V\cos\phi + P\sin\phi = 0$$

$$\circlearrowleft \sum M_1 = 0 \Rightarrow M - W\left(\frac{D}{2}\cos\alpha\right) - V\left[\frac{D}{2}\sin(90° - (\phi + \alpha))\right]$$
$$+ P\left[\frac{D}{2} + \frac{D}{2}\cos(90° - (\phi - \alpha))\right] = 0$$

unknowns: V, P, M

(3 eqns = ∴ 3 unknowns)

C.4

Strength Analysis (continued):

Solving, (assume $W = 20$ lbs., $\alpha = 32.6°$, $D = 56"$.)

$$\boxed{V = -\frac{W}{2}\cos\phi} \longrightarrow \text{@ } \phi = 0°, \quad V_{max} = -10.0 \text{ lbs.}$$

$$\boxed{P = \frac{W}{2}\sin\phi} \longrightarrow \text{@ } \phi = 90°, \quad P_{max} = 10.0 \text{ lbs.}$$

$$\boxed{M = \frac{D}{2}\left[W\cos\alpha + V\sin(90° - (\phi + \alpha)) - P(1 + \cos(90° - (\phi + \alpha)))\right]}$$

$$\text{@ } \phi = 0°, \quad M_{max} = 235.9 \text{ in-lbs.}$$
$$(P = 0)$$

Bending Stress,

$$\sigma_{max} = \frac{M_{max}C}{I} \longrightarrow \boxed{\sigma_{max} = 525 \text{ psi}}$$

Normal Stress

$$\sigma_{max} = \frac{P_{max}}{A} \longrightarrow \boxed{\sigma_{max} = 5.1 \text{ psi}}$$

Shear Stress

$$\tau_{max} = \frac{V_{max}Q}{Ic} \longrightarrow \boxed{\tau_{max} = 11.3 \text{ psi}}$$

Al. alloy, $\sigma_{yield} = 35,000$ psi

C.5

Actuator Power Requirements:
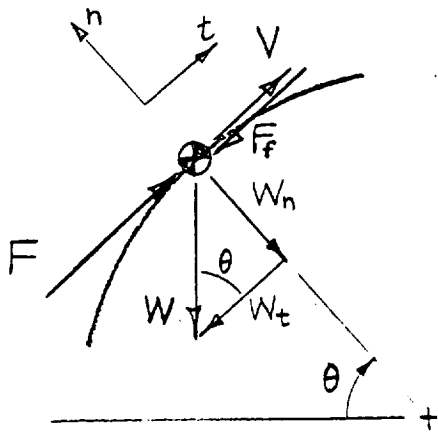
$F \Rightarrow$ Actuator force
$F_f \Rightarrow$ Friction force
$V \Rightarrow$ Tangental Velocity
$W \Rightarrow$ Load
$W_n \Rightarrow$ Normal Load
$W_t \Rightarrow$ Tangental Load
$\theta \Rightarrow$ Angle relative to horizontal

Assume:

1) No tangential acceleration; V is constant @ any θ
2) Require $V = 6\ ^{in}/_{sec}$
3) Kinetic friction force coefficient, $\mu_k = 0.2$
4) Neglect centripetal force

Find Actuator Force:

$$\Sigma F_t = 0 \implies F = W_t - F_f \qquad \text{where}$$

$$W_t = W \cos \theta$$

$$F_f = \mu_k W_n = \mu_k W \sin \theta$$

$$F = W \cos \theta - \mu_k W \sin \theta$$

$$\text{Power} = F \cdot V \longrightarrow \text{Power} = W(\cos \theta + \mu_k \sin \theta) V$$

Actuator Power Requirements (continued):

Insert known variables and convert units,

$$\boxed{\text{Power}(\theta) = 0.0182\,(\cos\theta + 0.2\sin\theta)\ hp}$$

Max Power Required (when $\frac{dP}{d\theta} = 0$)

$$\boxed{P_{max} = 0.0186\ hp, \quad @\ \theta = 11°} \quad (\sim 15\ \text{Watts})$$

Torque Requirements:

Basic
Eqn.:
$$P_{max} = T \cdot \omega \quad , \quad \omega \Rightarrow \text{Angular Velocity}$$

$$\omega = 6.0\ {}^{rad}\!/_{sec} = 57.3\ {}^{deg}\!/_{min}$$

(from prescribed rate)

$$P_{max} = 10.2\ \frac{ft\text{-}lb}{sec}$$

$$\therefore \boxed{T = 1.70\ ft\text{-}lbs. = 327\ oz\text{-}in.}$$

Final Dimension Analysis
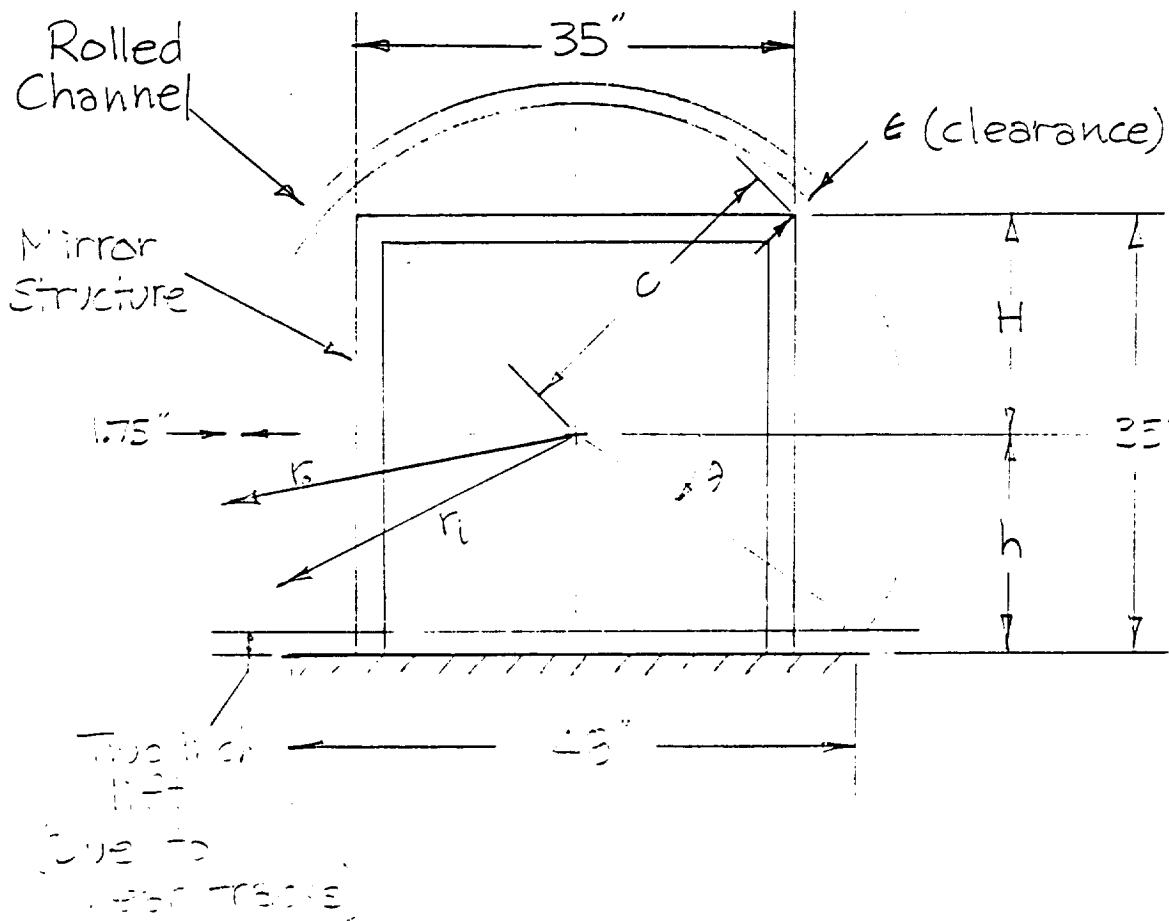
r_o (in.)	θ (°)	$h = r_o\sin\theta + 2''$	$H = 35'' - h$	$C = \sqrt{17.5^2 + H^2}$	$\epsilon = r_i - C$
28	31	16.42	18.58	25.52	+0.73
28.5	32.6	17.35	17.63	24.84	+1.91
28.25	31.8	16.9	18.10	25.18	+1.32
28.375	32.2	17.14	17.86	25.01	+1.61

A clearance of 2" is reasonable.

∴ choose $r_{outside} = 28.5''$

$r_{inside} = 26.75''$

C.8

Front

1/16 × 4

1/2 bearing × 2, 3/16 worm shaft

8/32

3/32

11/32

8/32

5/32

Bottom

7/32

5/8

1¼

4/16

¼

1
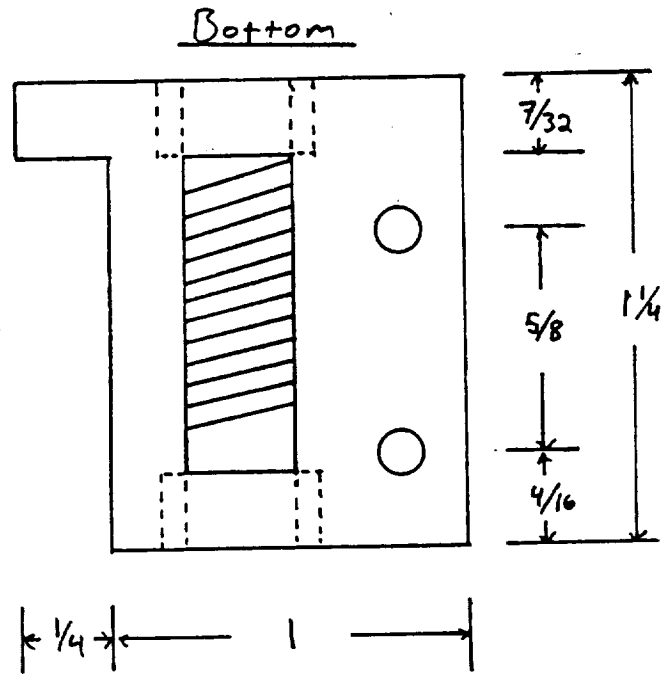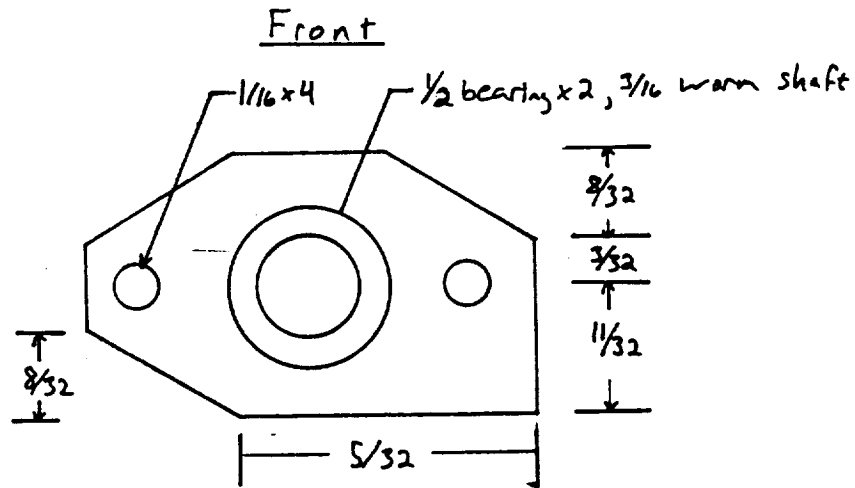
All dimensions in inches

Worm Gear Reducer
C.9

Front

½
hub

½ bearing

| 4/16 | 3/16 | ½ |

Top

1/16 × 2

3/16 shaft

| 4/16 hub | 5/32 | ½ |
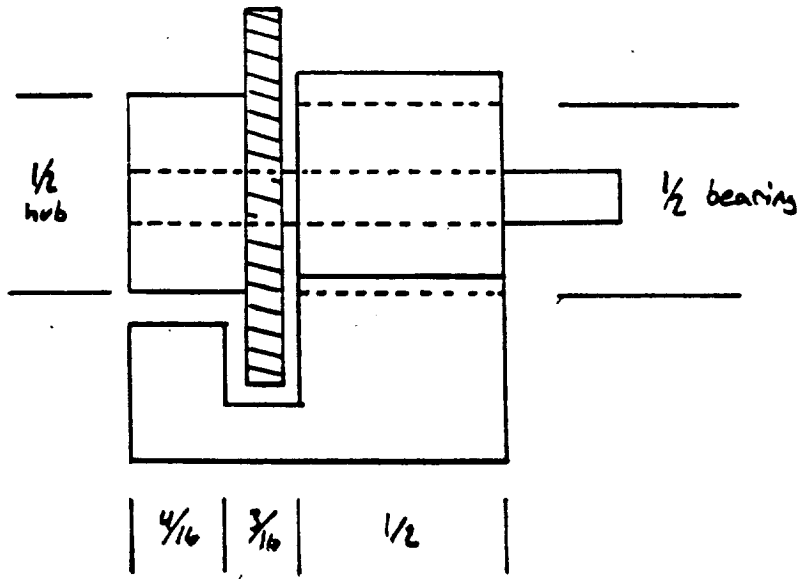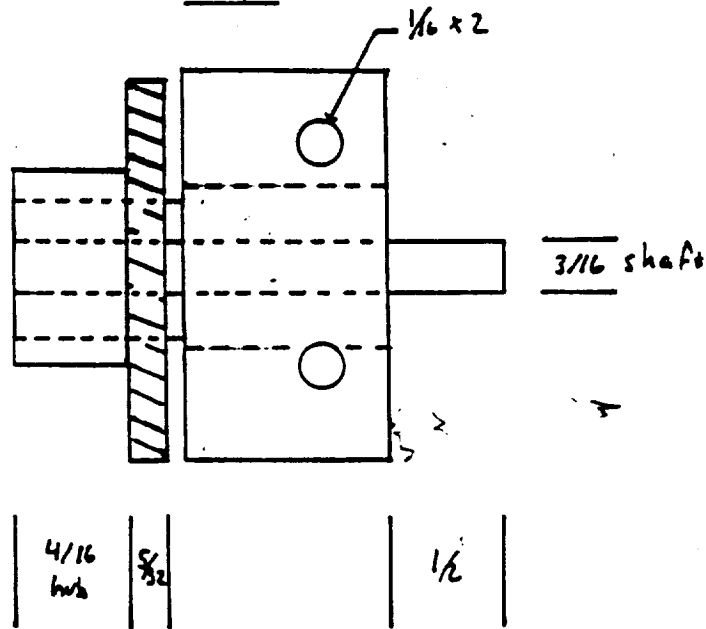
All dimensions in inches

Worm Gear Reducer

C.10

APPENDIX K

ELBOW JOINT

1 1/2 OD
1/8 wall

5/8

3/16

1 7/16

3 1/8

3/16

3/4

3

1/8 x 4
1 deep

7/8

FRONT

1

1/2

1 7/8

.873 ± .001
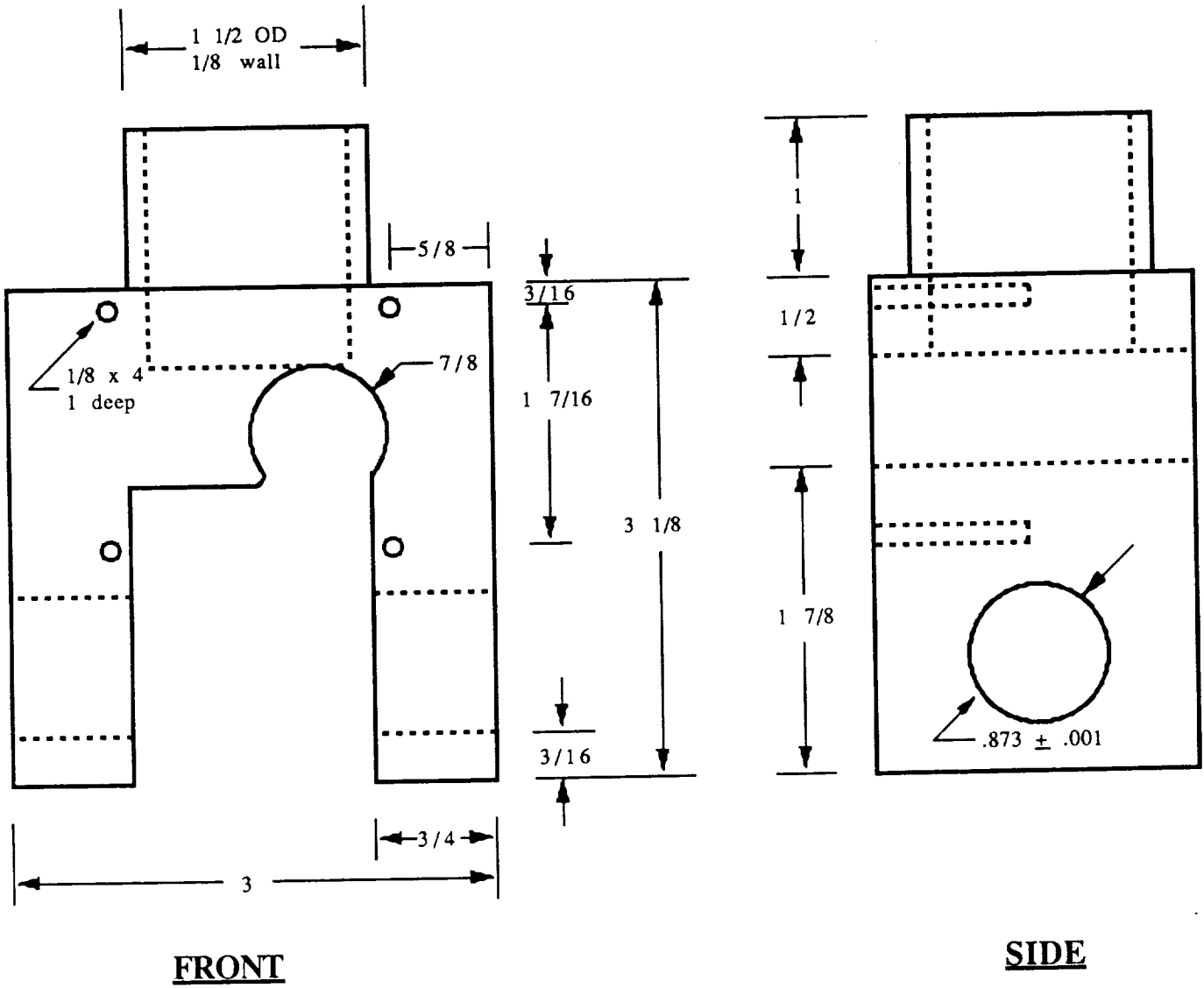
SIDE

All dimensions in inches

ELBOW JOINT

7/16 | 5/16

1/16

2 1/8

5/16

5/8

1

1 1/2 OD
1/8 wall
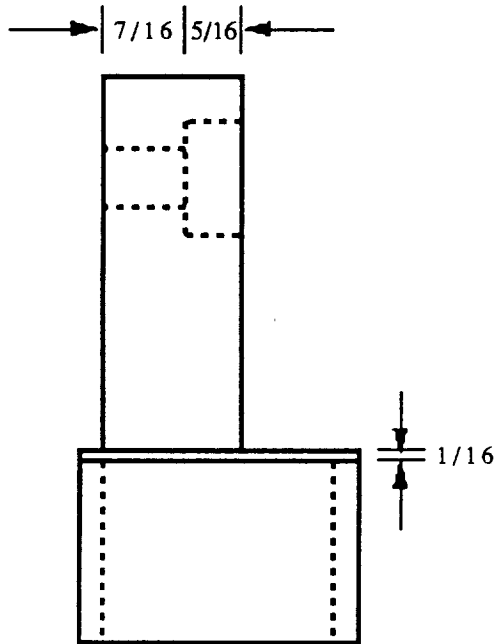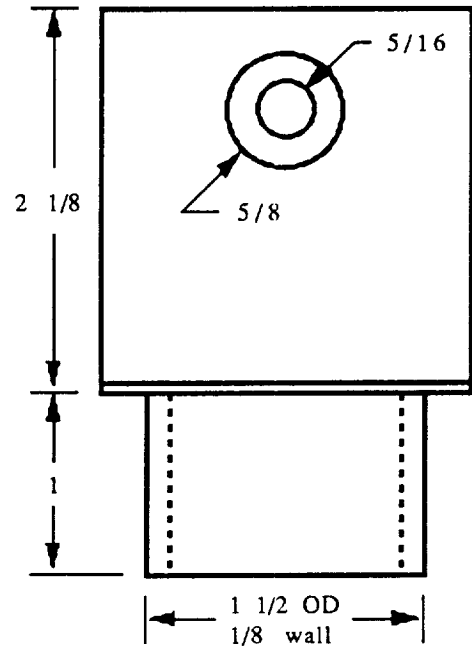
Front

Side

All dimensions in inches

APPENDIX L

MOTOR MOUNT

TOP

3/8 X 1/4 X 2

5/8

1/8

2

1/8 x 4

1/2

1/4

1 1/2

3/8

2/8

1
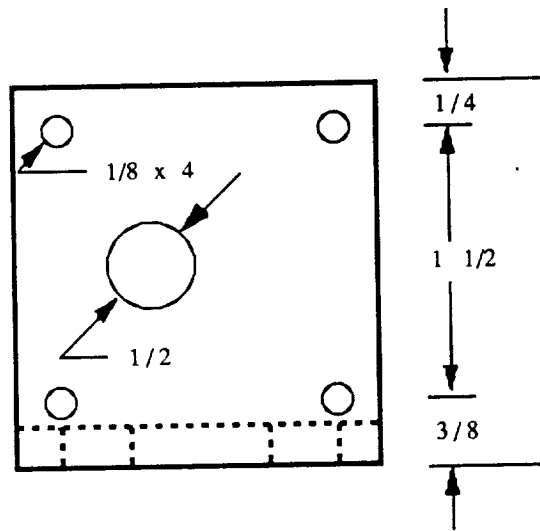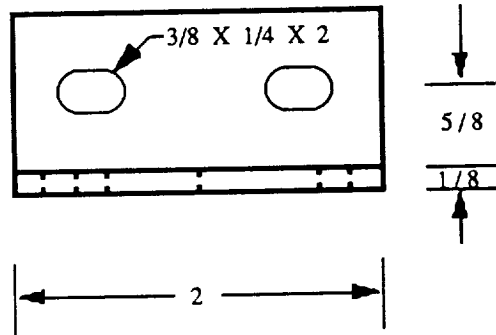
FRONT
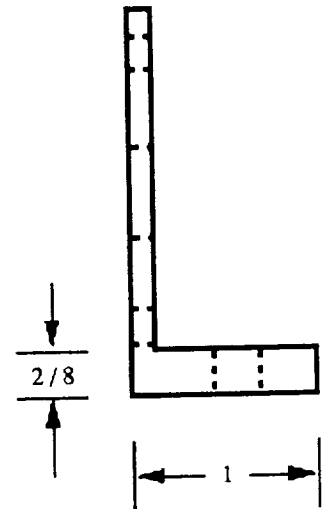
SIDE

All dimensions in inches
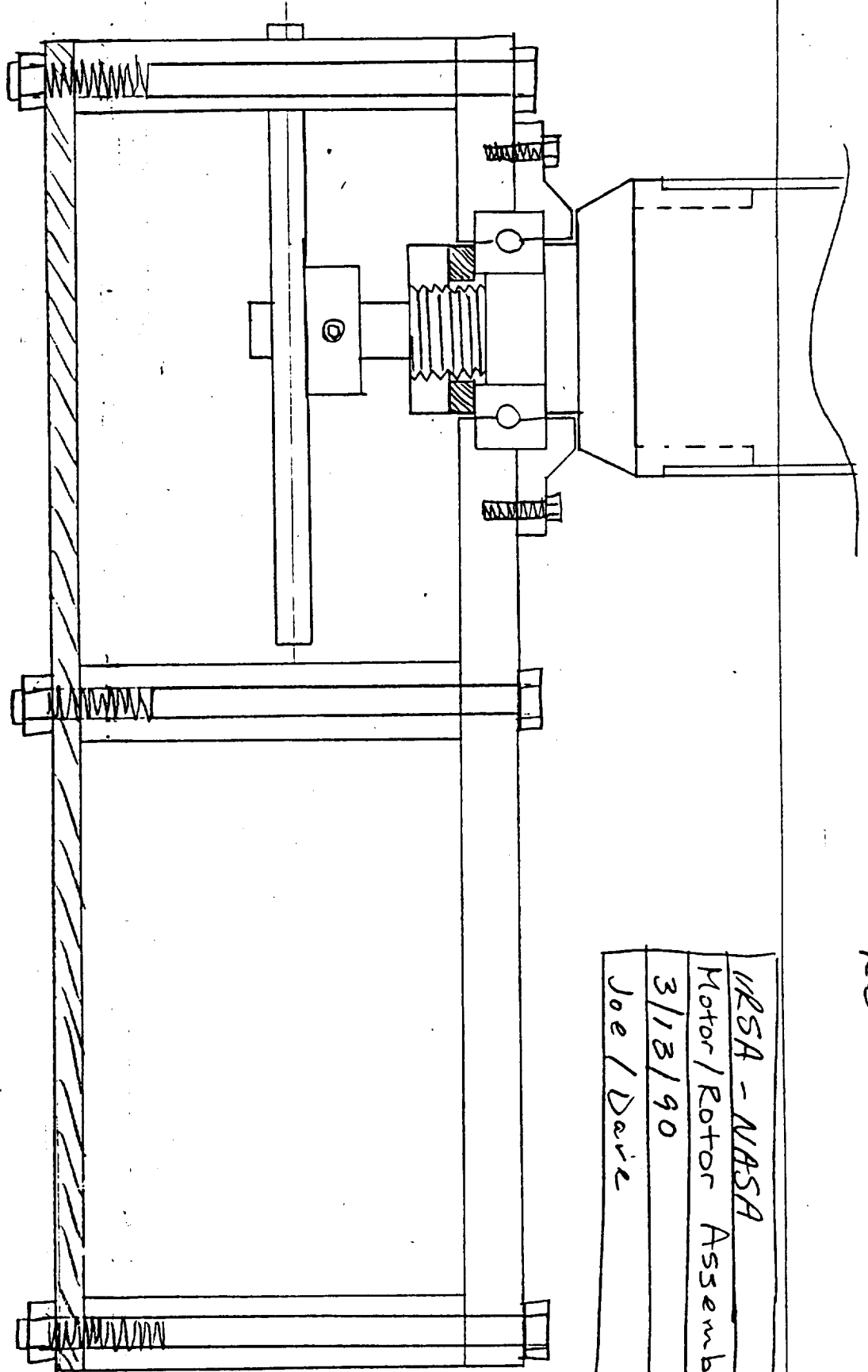
URSA-NASA
Motor/Rotor Assembly
3/13/90
Joe/Dave

Rev. D

Fig. D3

Pitch ⌀ 4.167"

$\frac{11}{16} = \tan 35°$

35°

9.000

4.000

.5

.5
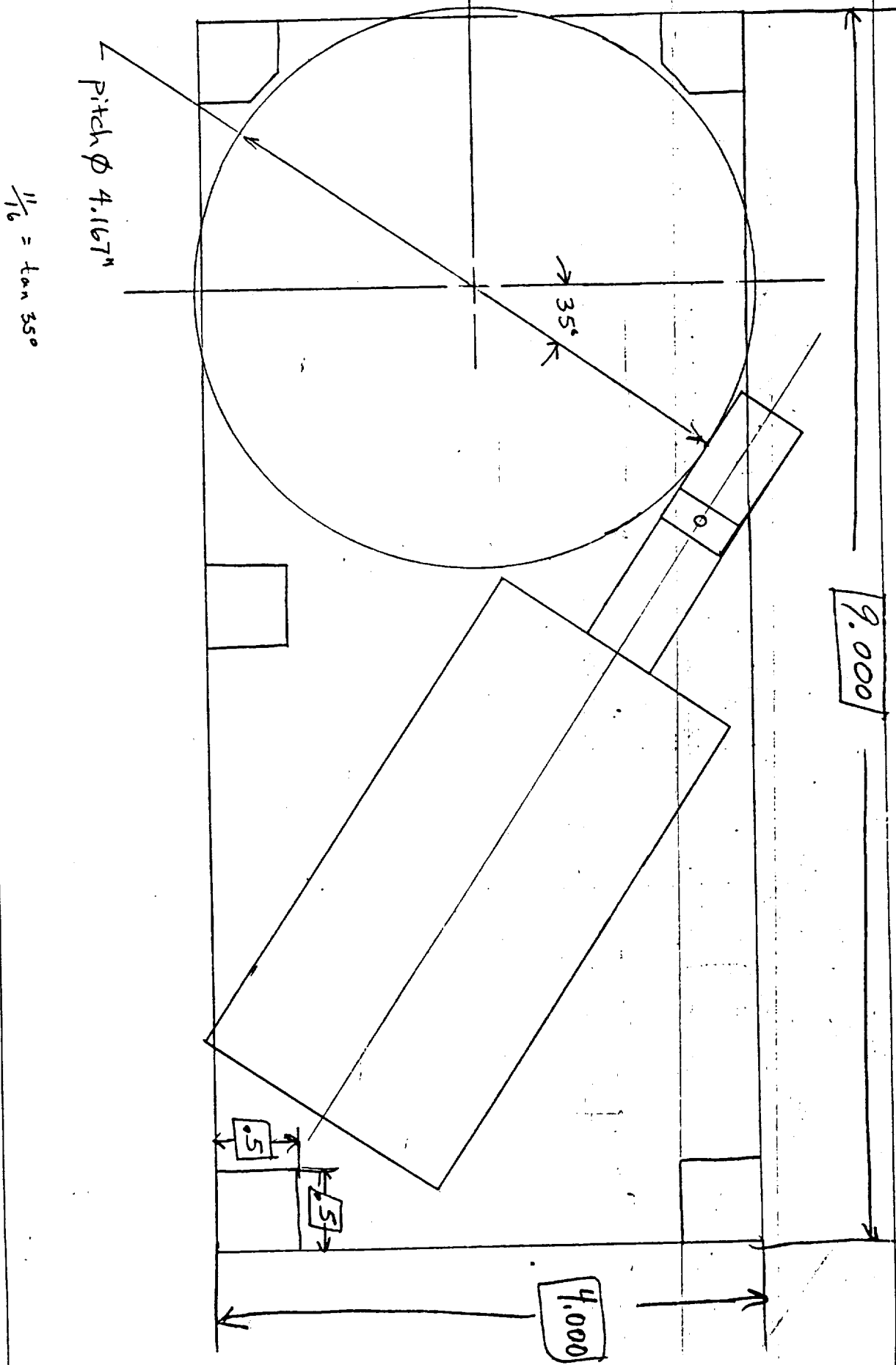
Rev. B

APPENDIX M

MANIPULATOR
Open position
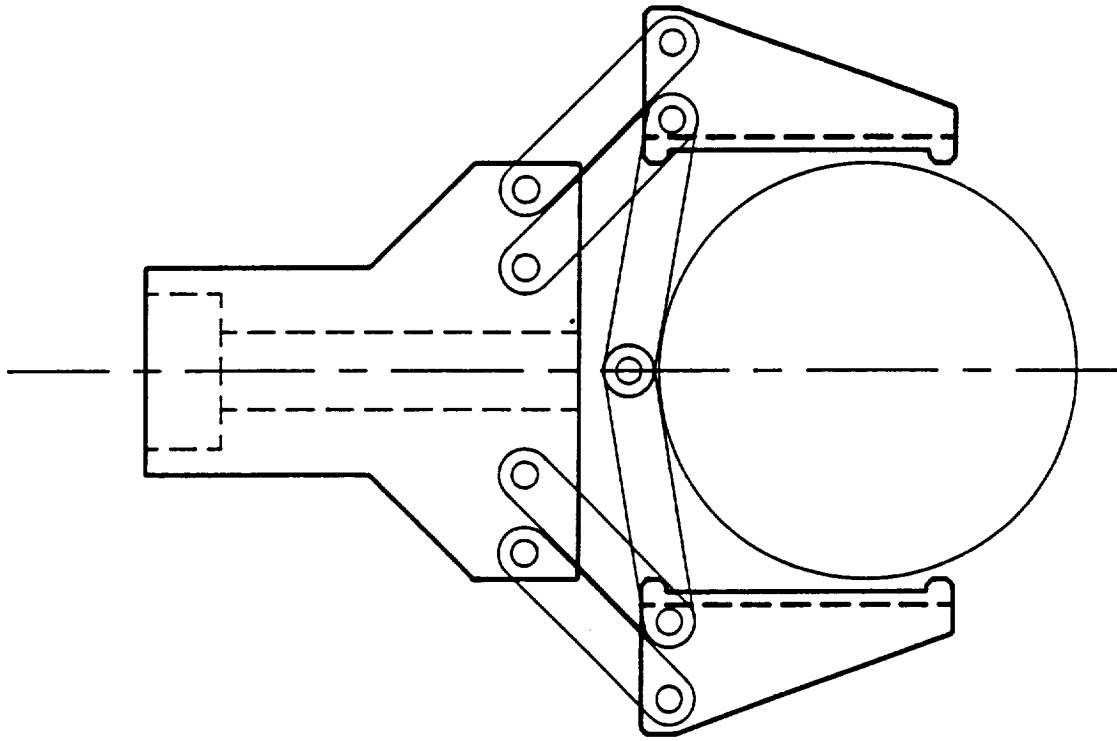
Figure 1

URSA - ROBOTIC ARM

MANIPULATOR
Closed position
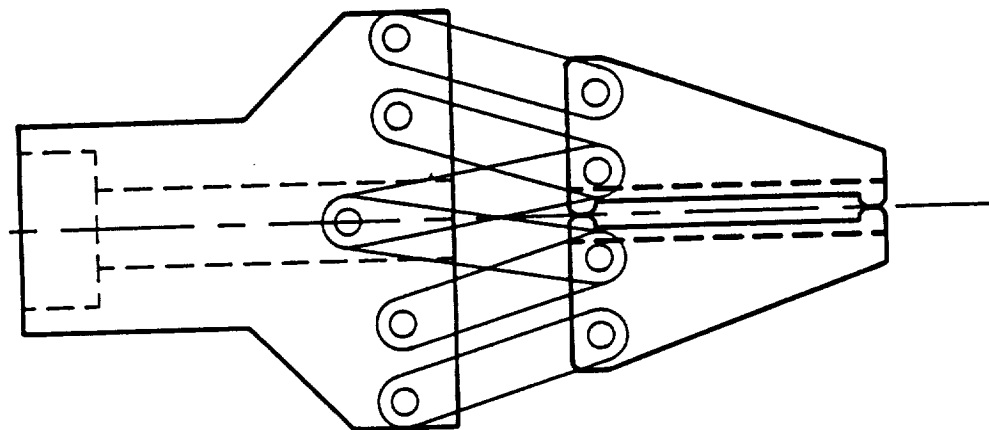
Figure 2
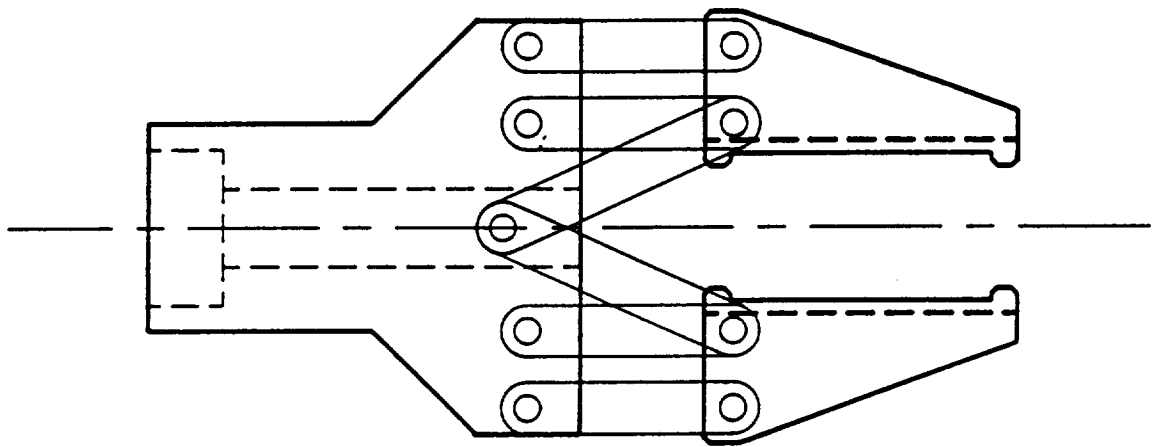
URSA - ROBOTIC ARM

MANIPULATOR
Intermediate position

Figure 3

URSA - ROBOTIC ARM
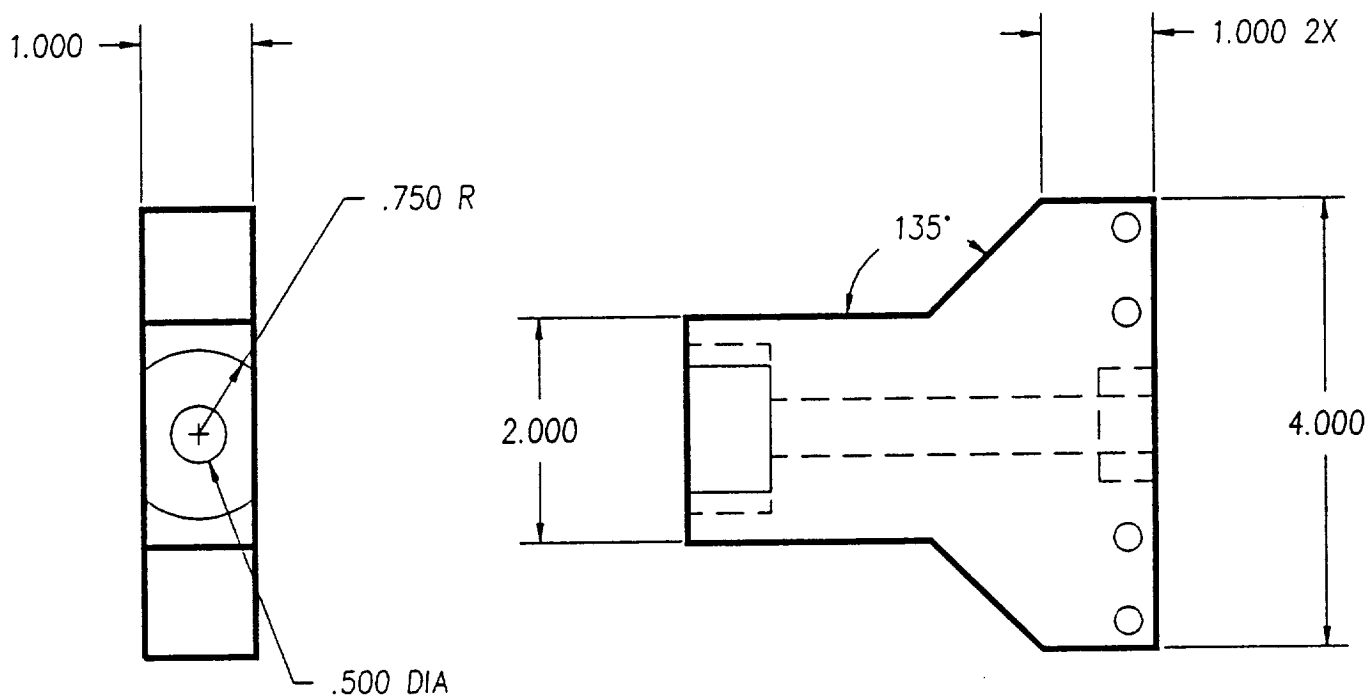
C-2

BASE DIMENSIONS
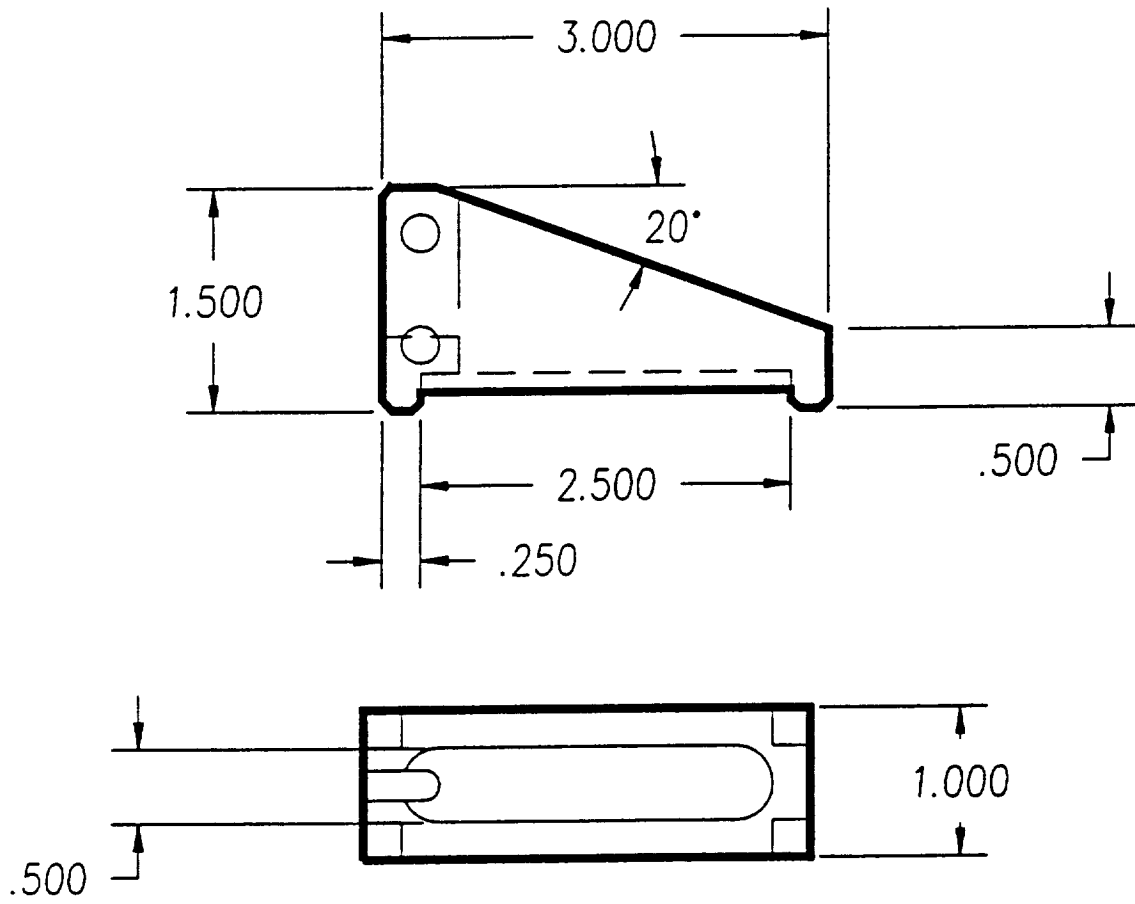

Figure 5

URSA - ROBOTIC ARM

GRIP DIMENSIONS

Figure 6

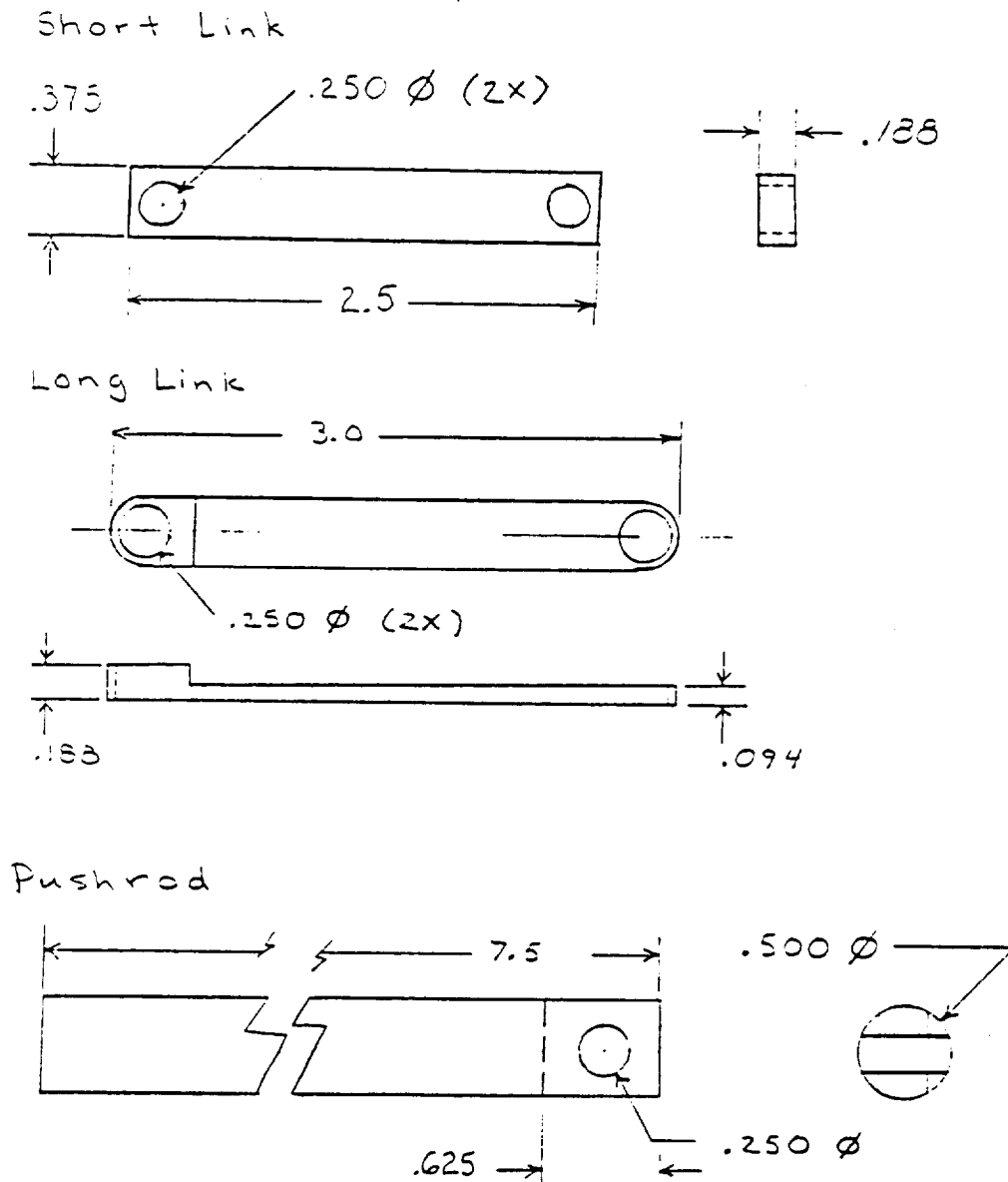**URSA - ROBOTIC ARM**

LINK, PIN, AND PUSHROD DIMENSIONS

Short Link

.375

.250 ∅ (2x)

.188

2.5

Long Link

3.0

.250 ∅ (2x)

.188

.094

Pushrod

7.5

.500 ∅

.625

.250 ∅

Figure 7

URSA - ROBOTIC ARM